This is a repository copy of *Advanced kinetic modelling strategies: Towards adoption in clinical PET imaging*.

White Rose Research Online URL for this paper:
http://eprints.whiterose.ac.uk/93618/

Version: Accepted Version

eprints@whiterose.ac.uk
https://eprints.whiterose.ac.uk/

Advanced kinetic modeling strategies: towards adoption in clinical PET imaging

Fotis A. Kotasidis[1,2†], Charalampos Tsoumpas[3], Arman Rahmim[4]

[1]Division of Nuclear Medicine and Molecular Imaging, Geneva University Hospital, Geneva, Switzerland

[2] Wolfson Molecular Imaging Centre, MAHSC, University of Manchester, Manchester, UK

[3] Division of Medical Physics, University of Leeds, Leeds, UK

[4] Department of Radiology, Johns Hopkins University, Baltimore, MD 21287, USA

Abstract

Positron emission tomography (PET) is a highly quantitative imaging modality and can probe a number of functional and biologic processes depending on the radio-labeled tracer. Static imaging followed by analysis using semi-quantitative indices, such as standardized uptake value (SUV), is used in the majority of clinical scans. However, considerably more information can be extracted from dynamic image acquisition protocols followed by application of appropriate image reconstruction and tracer kinetic modelling techniques. At the same time, this approach has been mainly restricted to drug development and clinical research applications due to their complexity both in terms of protocol design as well as methodology for parameter estimation. Active research in the field of non-invasive input function extraction, novel protocol design for whole body and dual tracer parametric imaging applications, as well as kinetic parameter estimation methods utilizing spatiotemporal (4D) image reconstruction algorithms aim to make this overall potentially more powerful approach more feasibly adopted in routine clinical imaging. Furthermore with the advent of sequential and simultaneous PET/MR, strategies for synergistic benefits in kinetic modelling are starting to emerge, potentially enhancing the role and clinical necessity of PET/MR imaging. In this article we elaborate and review different advancements in kinetic modelling both from a protocol design as well as the methodology point-of-view. Moreover, we discuss future trends and potentials which could facilitate more routine usage of tracer kinetic modelling techniques in clinical practice.

[†]**Corresponding author:**

Fotis Kotasidis, Ph.D
Geneva University Hospital
Division of Nuclear Medicine and Molecular Imaging
CH-1211 Geneva, Switzerland
Tel: +41 22 372 7257
email: fotis.kotasidis@unige.ch

1.1 Introduction

Positron emission tomography (PET) is a powerful and highly specialised imaging modality for non-invasive measurements of different physiological and biological processes at a molecular level. The theory of emission tomography applies to PET, but the data acquisition is significantly different from the well-known single photon emission tomography (SPECT). The principles of PET are based on the fact that by labelling a compound with a positron emitting isotope and intravenously injecting it in the patient in tracer quantities, one can detect its bio-distribution inside the body and investigate a number of physiological and biochemical processes such as perfusion, proliferation and glucose metabolism. The following discussion focuses mainly but not exclusively on [^{18}F]FDG PET imaging and is easily extendible to other tracers.

1.2 PET imaging in oncology

PET is an establish modality in Oncology, as for the last 2 decades PET imaging has been used for numerous studies, involving many benign and malignant abnormalities. One of the radiopharmaceuticals that is mostly used is [^{18}F]FDG or18-F labeled 2 deoxy-2-D-glucose. As FDG and glucose are similar, they compete during phosphorylation. The 2 byproducts FDG-6-phosphate and glucose-6-phosphate follow different routes. Glucose is further metabolized into fructose-6-phosphate, while FDG is trapped. The basis of [^{18}F]FDG PET is the elevated levels of glucose consumption in malignant cells. Increased expression of glucose transporters and enzymes responsible for metabolism can contribute to this glucose accumulation and consumption. FDG uptake is also regulated by the hypoxic nature of the tumor as well as the cellular proliferation and reduced tumor suppressing mechanisms [1].

The 2 tissue compartmental model can adequately describe the kinetics of FDG. The first compartment is the free tracer and the second one is the trapped FDG-6-phosphate. The tracer enters the free pool with a rate constant equal to K_1 which is the product of blood flow (BF) and extraction fraction (EF). In the case of FDG the EF is in the order of 20% and K1 reflects this EF. In the free pool the tracer can either be cleared with a rate k_2 and a fractional clearance rate ($K_1 k_2 / k_2 + k_3$) or become trapped with a rate k_3 and a fractional uptake rate ($K_1 k_3 / k_2 + k_3$) = Ki. The PET signal is decomposed into the input function and the impulse response function from the 2 compartments. The IRF from the free compartment can be considered as the input to the compartment K_1 multiplied by the exponential decay due to clearance or trapping $C_f = K_1 e^{-(k_2 + k_3)t}$. Accordingly the IRF for the bound compartment can be factorized as the input integral from the free compartment multiplied by the trapping rate

$$C_{b(t)} = k_3 \int_0^t C_{f(t)} dt = k_3 \int_0^t K_1 e^{-(k_2 + k_3)t} dt = \frac{K_1 k_3}{k_2 + k_3}(1 - e^{-(k_2 + k_3)t}) \quad (1)$$

The impulse response function can then be factored as:

$$C_{PET(t)} = C_{f(t)} + C_{b(t)} = K_1 e^{-(k_2 + k_3)t} + \frac{K_1 k_3}{k_2 + k_3}(1 - e^{-(k_2 + k_3)t}) = K_1 (e^{-(k_2 + k_3)t} + \frac{k_3}{k_2 + k_3}(1 - e^{-(k_2 + k_3)t})) = IRF$$

$$(2)$$

with the overall PET signal being the convolution of the IRF with the input function.

$$C_{PET(t)} = IRF \otimes C_{a(t)} = (K_1 (e^{-(k_2 + k_3)t} + \frac{k_3}{k_2 + k_3}(1 - e^{-(k_2 + k_3)t}))) \otimes C_{a(t)} \quad (3)$$
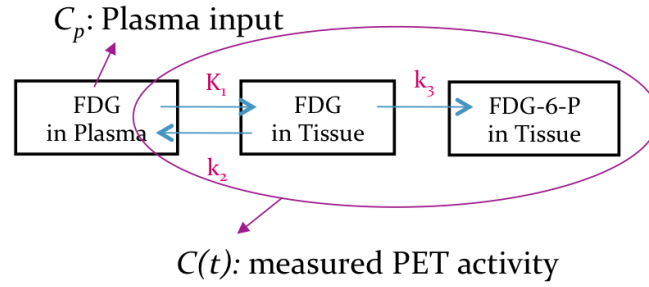
Fig 1. Two-tissue compartmental model. The interstitial space and cellular space are commonly lumped together as the first tissue compartment. K_1 and k_2 then capture delivery of FDG into and out of this compartment, and k_3 captures the intracellular phosphorylation rate. Measured PET signal C(t) cannot distinguish between non-phosphorylated and phosphorylated compartments.

1.3 Pitfalls in static clinical imaging - Why dynamic imaging ?

PET scanners are very specialized cameras and in principle work in a similar way to normal digital cameras, by collecting photons over a period of time, to produce a static image from the integrated measurements. This mode of imaging is almost exclusively used in clinical practice, for qualitative assessment and visual inspection and interpretation of the reconstructed images. However quantitative estimates related to the accumulation of a radio-labelled compound have complemented or superseded the visual interpretation in many clinical applications and provide a more objective assessment of the system under study.

Semi-quantitative indices such as the standardized uptake value (SUV) can provide valuable information regarding the system under study and can help in interpretation, differentiation and analysis, for tumour detection, staging and response monitoring. However tracer uptake values have also been used for other applications, such as measuring the extent of tumour oxygenation and angiogenesis, the level of tumour receptor expression and evaluating inter-tumoral uptake heterogeneity.

SUV is a simplified metric that requires single temporal-frame imaging:

$$SUV = \frac{\text{activity concentration } C(t)}{\text{Injected dose / Body weight}} \quad (4)$$

It is frequently used in oncology as a simple method of basic quantification in static imaging protocols and provide a surrogate estimate to biologically related parameters. The SUV can actually be viewed as an estimate of the kinetic influx rate K_i, and the accuracy in the estimation depends on the following two conditions:

(a) in the voxel or region of interest, contribution of non-phosphorylated FDG (which includes the vascular and the extravascular compartments) is negligible relative to phosphorylated FDG (a commonly utilized two-tissue compartmental model is shown in Fig. 1.

(b) time integral of plasma FDG concentration is proportional to injected dose divided by body weight (BW), lean body mass (LBM) or body surface area (BSA) as used in the SUV metric (the latter two are somewhat more reliable and less prone to artificial increase or decrease due to change in body habitus, e.g. as is common among oncology patients undergoing treatments [2-6].

These two assumptions can however break down in clinical PET imaging and lead to noticeable inaccuracies [7-10]. As for the first assumption, less FDG-avid tumours that have
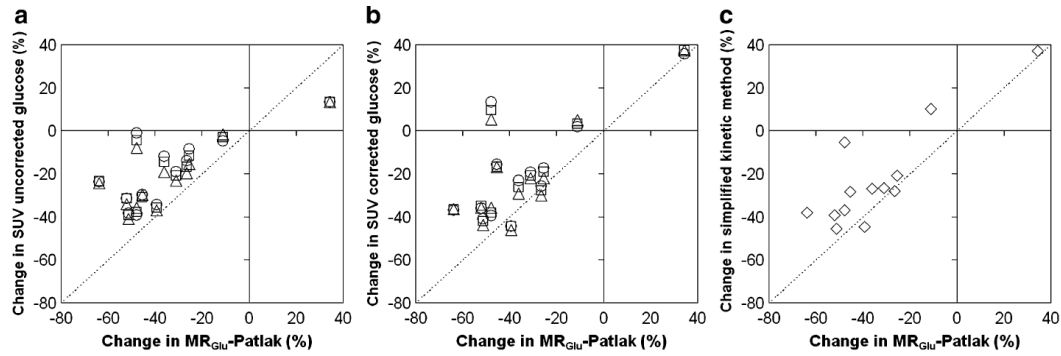
Fig 2. Relative percentage changes in SUV and SKM due to therapy compared with corresponding changes in MRGlu-Patlak on a lesion per lesion basis for SUVBW (triangles), SUVLBM (circles) and SUVBSA (squares) (a) uncorrected for blood glucose and (b) corrected for blood glucose, and (c) for SKM. All simplified method showed a substantially smaller fractional change than Patlak analysis, emphasizing the importance of kinetic analysis in assessing response to therapy [11].

relatively small FDG phosphorylation rates may not be optimally imaged at standard imaging times (e.g. 60min after injection) due to contributions of the vascular compartment and/or intracellular non-phosphorylated FDG, thus resulting in limited differentiability between diseased and normal tissue or organs [12]. This can be a particular issue post-therapy when there can be substantial background FDG activity in tissues [13]. This also leads to spatial distributions for SUV images that vary with time (a special problem in practice due to variable scan times post injection inherent in clinical practice).

As for the second condition, if a patient is for instance undergoing chemo- or hormone therapy, the dynamics of plasma FDG could be significantly affected, and the time integral of the plasma FDG could deviate from what would be predicted from the dose and BW/LBM/BSA alone [9, 14]. The SUV estimate for such a case could then not accurately correspond to the kinetic influx rate, and the therapy response may not be accurately reflected by the change in SUV. This latter also explains why patient populations of varying plasma dynamics result in scattered correlation between the SUV and K_i measures [15].

Overall, the single time point SUV PET/CT methodology has documented limitations (e.g. [16-21]) in terms of separation between malignant uptake and benign uptake (e.g. inflammation, infection), and may underestimate disease presence in certain malignancies [7]. A more advanced approach, namely dual-time-point FDG PET imaging proposes to measure the retention index (RI) as the percent change in SUV images from early (~60 min) to late (90 to 180 min) scans [22-31]. This approach has been applied to a number of malignancies; e.g. head and neck [32], lung [33], breast [34], gallbladder [35], cervix [36] and glioma [37], and has been shown to result in enhanced differentiation between malignant vs. benign processes [32, 38, 39] and improved prognostic utility [40]. At the same time, RI is also a semi-quantitative measure of tissue or tumor FDG kinetics. For a fixed system of micro-parameters, it can (undesirably) modulate (i) with different temporal positioning of the dual scans and (ii) with varying plasma dynamics. Moreover, this technique can require long patient waiting times and may face increased likelihood of misalignments (and difficulty in correction) between early and late scans.

In a treatment response monitoring study by Freedman et al. [41], it was demonstrated that changes in the SUV did not correlate well with K_i, and in some cases generated "large" discrepancies resulting in opposite conclusions regarding the progression of disease. The authors attributed the discrepancies to the above-mentioned two shortcomings of the SUV measure. A solution to the second shortcoming is to supplement the PET scan with blood sampling data, arriving at the fractional uptake rate (FUR) measure [42, 43]. This approach in its original form involved invasive blood sampling from time of injection. A closely related approach, referred to as simplified kinetic analysis (SKA), utilized population-based input

4

functions, and blood sample collected late-phase to scale the population-based input function [44]. In any case, the FUR/SKA approaches, similar to the SUV framework, continue to not correct for the presence of nonphosphorylated FDG. In fact, it was shown in [41] that although merely correcting the SUV for the available plasma input did somewhat improve correlations between changes in SUV and K_i (from 0.733 to 0.849), it only minimally reduced number of "large" discrepancies between the two measures. Additional correction of the SUV for contributions of nonphosphorylated FDG resulted in excellent correlation (0.975) and zero large discrepancies, exposing the deficiencies associated with single time frame imaging. In a comparative study Cheebsumon et al found that fractional changes in assessing response to therapy were under- or over-estimated using SUV compared to Patlak analysis (Fig 2) even after correcting for plasma glucose levels [45]. Several studies have compared a number of semi-quantitative methods based on static protocols (SUV, simplified kinetic method) with kinetic analysis method based on dynamic imaging protocols (Patlak graphical analysis and full compartmental modelling) on [^{18}F]-FDG imaging, further motivating the need for dynamic imaging [46-49].

When dynamic methods are used, the individual rate constants have to be calculated using multiple time courses of the activity concentration in the tissue of interest. Two deferential equations can describe the concentration change rate in each compartment to analytically derive the operational equation.

$$\frac{dC_{f(t)}}{dt} = K_1 C_{a(t)} - k_2 C_{f(t)} - k_3 C_{f(t)} + k_4 C_{b(t)} \quad (5) \qquad \frac{dC_{b(t)}}{dt} = k_3 C_{f(t)} - k_4 C_{b(t)} \quad (6)$$

After using Laplace transformations the compartmental concentrations can be written as

$$C_{f(t)} = \frac{K_1}{a_2 - a_1}((k_4 - a_1)e^{-a_1 t} + (a_2 - k_4)e^{-a_2 t}) \otimes C_{a(t)} \quad (7) \qquad C_{b(t)} = \frac{K_1 k_3}{a_2 - a_1}(e^{-a_1 t} - e^{a_2 t}) \otimes C_{a(t)} \quad (8)$$

And the overall PET signal as

$$C_{PET(t)} = \frac{K_1}{a_2 - a_1}((k_3 + k_4 - a_1)e^{-a_1 t} + (a_2 - k_3 - k_4)e^{-a_2 t}) \otimes C_{a(t)} \quad (9)$$

where

$$a_1 = (k_2 + k_3 + k_4 - \frac{\sqrt{(k_2 + k_3 + k_4)^2 - 4k_2 k_4}}{2}) \quad (10)$$

$$a_2 = (k_2 + k_3 + k_4 + \frac{\sqrt{(k_2 + k_3 + k_4)^2 - 4k_2 k_4}}{2}) \quad (11)$$

The metabolic rate of glucose can then be calculated as $MRgl = \frac{C_p}{LC} \frac{K_1 k_3}{k_2 + k_3}$ with the lumped constant (LC) being the difference in transport and phosphorylation between glucose and FDG and C_p the arterial plasma glucose concentration.

1.4 Clinical indications for pharmacokinetic modelling

The last few years a number of studies have highlighted the potential role of kinetic modelling in diagnosis, by providing addition parameters more relative to the underlying pathology, while at the same time assisting in drug development and therapy response monitoring through drug labelling and subsequent kinetic parameter evaluation.
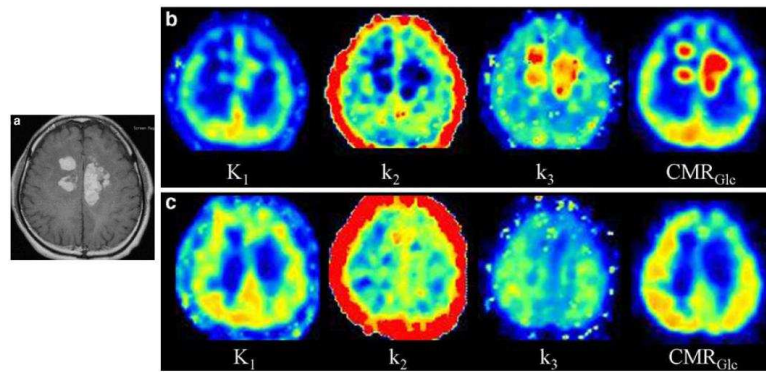
Fig 3. MR and FDG PET images in a 47-year-old male patient with diffuse large B cell CNS lymphoma. Contrast T1-weighted MR image shows multiple enhancing lesions at bilateral paraventricular area (a). Baseline dynamic FDG PET shows an increase in K_1, k_3 and CMRGlc and a decrease in k_2 at lymphoma lesions (b). Follow-up dynamic FDG PET shows a decrease in all four parameters (c) [50].

The potential benefit of kinetic analysis has been demonstrated for a number of tracers and in a number of different pathologic conditions. In head and neck imaging and specifically in central nervous system lymphomas, kinetic analysis of dynamic [18F]-FDG may help in diagnosis as well as response monitoring (Fig. 3) [51, 52], while can provide more reliable tumour detection estimates [53]. Using [18F]-DOPA Schiepers et al [54] demonstrated the importance of kinetic modelling in tumour-grade differentiation, while Thorwarth et al [55] using [18F]-FMISO showed a high correlation between kinetic parameters and response to therapy. Similar findings have been reported by Schiepers et al [56] using [18F]-FLT in brain tumours, with a correlation between kinetic parameter estimates and disease progression while Wardak et al [57] in their study using glioma patients pointed out the significance of full kinetic modelling in therapy response monitoring. In lung cancer, dynamic [18F]-FDG imaging followed by kinetic analysis has been shown to assist in differentiation between squamous cell carcinoma, adenocarcinoma with differences in kinetics between these subtypes [58]. In colorectal tumours, kinetic analysis may help differentiate between primary tumours and normal tissue [59], while kinetic parameters may provide information with respect to proliferation and angiogenesis [60, 61]. Improved treatment monitoring and survival prognosis has also been demonstrated using information following kinetic parameter estimation [62]. Improved tumour differentiation has also been reported in soft tissue tumours [63, 64] while the importance of kinetic modelling in predicting the response to therapy has also been demonstrated [65]. A multitude of studies are available in the literature for the potential significance of kinetic modelling in clinical oncology and drug development as highlighted in a number of critical reviews [66-69].

1.5 Challenges in clinical adoption of pharmacokinetic modelling

The added benefit of kinetic modelling approaches compared to semi-quantitative indices have been reported in several studies. Fully quantitative analysis can provide more meaningful parameters compared to semi-quantitative indices, in term of their relation with the true physiological parameters that one is trying to infer. Traditionally though application of dynamic imaging protocols followed by graphical analysis or full kinetic analysis modelling strategies, has mainly been restricted to clinical research. The limited adoption of dynamic imaging protocols in clinical practice stems from the technical difficulties associated with kinetic modelling, rendering such techniques difficult to be adopted in routine clinical practice.

One of the main issues associated with clinical adoption of kinetic modelling is the need to have an accurate estimate of the tracer's activity concentration in the blood over the course of the dynamic study. Having an arterial input function using continuous blood sampling is the gold standard; however it is invasive, time consuming and technically challenging, while extensive facilities and specialized personnel are required. Alternatives are available and advancements in data processing, algorithmic design, instrumentation and multimodality imaging with PET/MR can facilitate in the routine extraction of input functions in the clinic.

Another important issue is the limited anatomical FOV coverage offered by current PET systems (15-25cm), restricting dynamic acquisition protocols to a specific part of the body. Therefore kinetic modelling strategies have so far been limited to single bed acquisition protocols, making them ill-suited for whole body parametric imaging applications. Furthermore dynamic imaging protocols can last for up to 1.5 hours post-injection and as such, affect both patient comfort, as well as patient throughput. However the recent introduction of novel data acquisition schemes for whole-body dynamic imaging coupled to improvements in scanner data acquisition and management, has enabled the early application of kinetic modelling strategies in whole-body clinical applications.

Choosing the correct model is very important and is dependent upon the administered tracer, the target region and the scanner characteristics. In most cases the actual underlying model is too complicated to be identified due to the statistical variations of the measured data and the limitations introduced by the instrumentation. A simplified version of the model is then chosen in most cases as a trade off between statistical reliability of the derived parameters and error due to using a simplified model. Furthermore, due to the limited counting statistics, parameter estimation is usually performed at a regional level, after ROI delineation based on anatomical information and kinetic model application. This method is attractive as many voxels are summed together, improving the statistics and resulting in reliable parameters. However as the underlying tissue contains heterogeneous kinetics, the average that is calculated when estimating regional kinetics, inheritably results in biased estimates. Additionally, the spatial average limits the spatial information that PET data can potentially provide. To overcome these problems, one should model the kinetics at the scanner's finest image discretization element, which is the voxel. In this way parametric images are obtained, allowing the spatial heterogeneity of the physiologic parameters to be assessed. However, despite the benefits of parametric imaging compared to regional analysis, it suffers from increased noise due to reduced counting statistics at the voxel level. This results in bias and non-statistically reliable parameter estimates. Also computational time becomes an important parameter. To address the excess noise, while maintaining the spatial information, different post reconstruction methods have been reported in the literature to improve signal-to-noise ratio (SNR), such as spatial and temporal filtering, Fourier transformations, ridge regression methods, spatial constraints and voxel clustering. These methods are expected to improve parameters but kinetic parameter estimation is performed using independently reconstructed images leading to suboptimal parameter estimation. Direct 4D parameter estimation methods provide a promising alternative but until recently their slow convergence properties and their added complexity have hampered their more frequent application. Novel optimization strategies for fast and efficient parameter estimation could render 4D reconstruction strategies suitable to be used in clinical dynamic imaging and provide parametric images of improved accuracy and precision.

1.6 Advanced strategies in pharmacokinetic modelling

As mentioned previously, there are a number of challenges associated with the clinical adoption of kinetic modelling strategies in clinical practice. However the last few years advancements in data analysis, protocol design and instrumentation have provided a solid
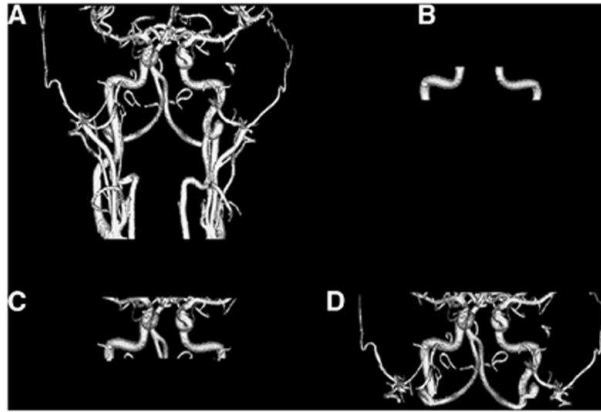
Fig 4. Three-dimensional rendering of segmented artery from the time-of-flight magnetic resonance angiography images (A); the arterial region of interest (ROI) version one (B); the arterial ROI version two (C); and the arterial ROI version three (D). Reprinted with permission from J Cereb Blood Flow Metab. Jan 2013; 33(1): 115–121.

foundation toward more widespread utilization of dynamic imaging followed by fully quantitative analysis, in the clinic. In the rest of the article we review techniques and recent advancements in key areas associated with pharmacokinetic modelling and discuss their potential application in routine clinical practice.

1.6.1   Input function estimation

Kinetic imaging requires the accurate calculation of the input function. Arterial blood sampling is an invasive and complicated method which makes scanning very uncomfortable to the patient and virtually impossible to translate in clinical practice. For this purpose, numerous techniques have been proposed to calculate the input function from images as a convenient and non-invasive alternative to arterial cannulation. However even image-derived input function (IDIF) estimation is by no means any easy task and there are several issues that needs to be addressed if such a methodology is to be applied in clinical practice. Here we list only some of them while a recent review article on IDIFs can be found by Zanotti-Fregonara et al [70].

- Segmentation of blood pool: One of the difficult aspects is to locate the region of interest with relevant information, e.g. carotid arteries. Many researchers have attempted segmentation of regions using the early time frames of the dynamic PET images. This is very difficult as PET resolution is limited to about 4-5 mm making the segmentation of small structure a difficult task. A way to solve this issue is to segment the arteries using angiograms acquired from other imaging modalities as shown in Fig. 4 [71]. For example, Fung and Carson have recently proposed of a method that used a particular MR protocol to obtain high resolution of the carotid arteries [72]. This technique along with another recent investigation by Iguchi et al [73] are promising examples to translate in the recently developed simultaneous PET/MR imaging. In cases of whole body imaging, this might be further complicated compared to brain imaging, due to additional sources of motion. A region, which could be used for obtaining the blood pool, is the cardiac cavity or ascending aorta, however this is generally limited to acquisitions that include these structures within the field of view.
- Limited Spatial Resolution: Dynamic PET imaging has limited spatial resolution due to partial volume and motion effects. In brain imaging, motion is relatively simple to correct by applying frame-by-frame realignment or measuring rigid motion with the use of external devices [74]. As such the main effect for limiting resolution is partial

volume, with activity spilling in and out. For example, Fung and Carson attempted to minimise this complication by selecting only a centreline [75]. On the other hand, in whole body, respiratory motion is a major challenge as it can degrade resolution for up to 2cm and it is the main limiting factor for quantitative imaging [76]. Motion correction approaches have been proposed using PET-MR imaging but such approaches are still at an early stage [77] and will require further work to translate them in the clinical PET-MR protocols. However in the body, since the regions used to extract the input function are relatively large compared to the carotids in the brain, partial volume effects can be less of a concern.

- Plasma Vs whole blood and metabolites: Even if the input function is calculated, there is need in several cases to calculate the amount of metabolites in the blood as they augment the background signal without necessarily participating in the kinetics, although in some cases metabolites may show competitive kinetics in some organs as discussed previously [78]. Luckily though in $[^{18}F]$-FDG imaging no metabolite correction is needed, while the difference between plasma and whole-blood concentration is minimal.

- Limited Temporal Resolution: PET in theory offers very high temporal resolution (less than a nanosecond) but in practice the spatiotemporal resolution is limited by the fact that enough counts need to be measured within a timeframe to extract quantitative information. Particularly, for the calculation of the peak of the input function a temporal resolution of a couple of seconds is needed. Current iterative reconstruction algorithms have the ability to provide high spatial resolution images but within this timeframe they fail to produce quantitative results due to noise-induced bias generated from the non-negativity constraint [79]. Furthermore using graphical analysis methods (such as Patlak) where the area under the input curve is important and for tracers with metabolites mainly at the late frames, the coarse sampling in the early frames, where the activity changes rapidly, will introduce errors in the subsequent kinetic parameters. This is due to the approximately estimated area under the peak (AUP) being a significant proportion of the total area under the curve (AUC) following metabolite correction compared to a non metabolized tracers, where the area AUP is only a small fraction of the AUC [80].

In particular cases that some regions in the brain exhibit simple and well-understood biochemical exchanges with the arterial input function, the kinetic parameters of the brain can be expressed by relating to the kinetic behaviour of this reference region [81]. These models are known as reference tissue models and have proven valuable for kinetic analysis of dynamic PET imaging of the brain function. However, the models are susceptible to a suitable reference tissue, which might not be apparent across a large range of patients and it is limited to particular tracers. Other methods, known as population-based input function, estimate the input function from a library of input functions [82].

Overall the translation of input function to whole-body parametric imaging is dependent on the tracer, the clinical application and the organ is imaged. There will be need to reconsider approaches currently in use, such as the IDIF methods and make them more robust by incorporating the power of new multimodality imaging techniques such as PET/MR as will be further elaborated.

1.6.2   Towards dynamic whole-body parametric imaging

Dynamic PET imaging has so far been primarily treated (incorrectly) as mutually exclusive from whole-body imaging. Both are very powerful, as we discuss below, and can be merged. This may have important implications in the clinic, including therapy response assessment,

and in phase-1 type studies involving new treatments, which commonly involve subjects with disseminated disease. The subsequent discussion and analsis primarily focuses on [^{18}F]-FDG PET imaging, but is also applicable to other tracers. Whole-body PET/CT imaging [83-87] is nowadays widely and routinely used for assessment of loco-regional and distant metastatic disease involvement. At the same time, PET can be used to quantitatively measure the FDG uptake or influx rate constant K_i (as surrogate of metabolic uptake) via dynamic imaging and tracer kinetic modelling [88-94] (the Patlak graphical method being commonly invoked in single-bed imaging). However, routine clinical multi-bed PET imaging commonly involves single temporal-frame imaging.

Clinically feasible combination of whole-body and dynamic imaging first poses the following challenges: (i) presence of temporal gaps for any given bed position, and (ii) need for non-invasive quantification of the input function, for clinical feasibility. The first one is addressed via graphical Patlak analysis, which can be applied with as little as two time point measurements. The second issue however is challenging, and we discuss shortly.

A particular study by Ho-Shon et al. [95] proposed optimization of multi-bed dynamic PET acquisitions, based on a statistical Bayesian regression method. This approach focused on ROI-based parametric analysis and included demonstration of 2-bed acquisition examples with uneven bed frames and bi-directional scanning. Similarly, in an abstract by Hoh et al. [96], multi-bed dynamic acquisition was proposed to allow for ROI-based Patlak analysis over multiple beds. Later, Sundaram et al. [97] motivated by the previously-mentioned SKA method, and also utilizing the suggestion by Hoh et al., proposed a short 2- or 3-bed late dynamic acquisition as a simplified alternative to multi-bed Patlak analysis aimed at ROI-level parametric analysis. Kaneta et al. [98] also conducted multi-bed dynamic acquisition of human subjects (0-90min post-injection) in the context of imaging hypoxia using ^{18}F-FRP170, involving multi-pass whole-body acquisitions, each lasting for 12min (6 beds x 2min/bed). However, only dynamic images were presented, without tracer kinetic modeling.

The Patlak model involves time-integral of the input function. A novel work by van den Hoff et al. [99] proposed a solution beyond this. Utilizing whole-body dual time-point image acquisition, and denoting $C(t)$ and $C_p(t)$ as the measured PET activity for a given voxel and the input function from the heart, respectively (as seen in Fig. 1), each measured at times t_1 and t_2, the authors showed that the Patlak slope K_i is estimated as:

$$Ki \approx \frac{1}{\sqrt{C_p(t_1)C_p(t_2)}} \frac{C(t_1)-C(t_2)}{t_2-t_1} + \frac{\bar{V}}{\frac{t_2-t_1}{\ln(C(t_1)/C(t_2))}} \quad (12)$$

where $\bar{V}$ denoted a population-based estimate of the Patlak intercept. The derivation included assumption of mono-exponential decay of the input function between the two scans. The results indicated excellent correlation (r=0.99) with actual Patlak measured slopes, and even when the second term in above equation was dropped (r=0.98) though in this case, the slope of regression changed substantially from zero. This approach was primarily validated using single-bed imaging (n=9), but also included application to a single whole-body scan.

Recently, another whole-body PET imaging scheme was proposed in companions papers by Karakatsanis et al. [100, 101], including optimization and validation. The approach involved 6min initial scan over the heart, as well as generation of dynamic whole-body datasets (6 passes), the latter shown in Fig.5. This enabled a non-invasive solution to input function estimation combining the first 6min scan over the heart (capturing the early dynamics) and subsequent passes over the heart. Standard Patlak linear graphical analysis modeling was employed at the voxel level, coupled with plasma input function estimation from the images, to estimate the tracer uptake rate K_i (slope), resulting in parametric images at
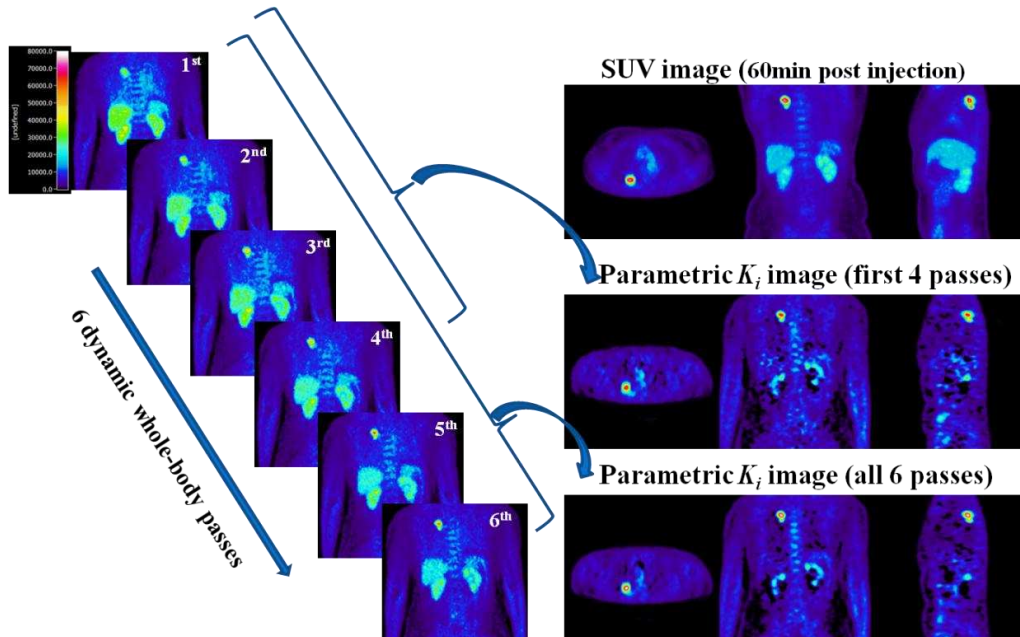
Fig 5. (left) Following 6min scan of the heart (not shown), 6 whole-body passes are acquired as shown. Every pass consisted of 7 bed positions (45sec/bed acquisition). (right) The SUV image, the K_i parametric image derived from all 6 last frames and the K_i image after omitting the last 2 frames are shown. Reprinted with permission from Karakatsanis et al., Phys. Med. Biol., vol. 58, pp. 7391-7418, 2013 (IOP Publishing).

the individual voxel level. The images (as seen in Fig.5) convey a different 'feel' compared to SUV imaging, for instance saturating background FDG activities as commonly seen in some organs (e.g. liver has considerable blood presence). A similar acquisition approach was recently investigated by another group for n=21 patients with malignant or benign pulmonary lesions [102] showing good ability to distinguish malignant lesions from benign ones (p<0.05), though a similar statistical significance was observed when utilizing SUVmax. The abovementioned framework was also recently extended using a generalized Patlak model that additionally incorporates modeling of FDG dephosphorylation (k_4 constant) [103].

This framework, however, faces a number of challenges:

(a) It can result in enhanced noise levels. To address this, two general solutions may be explored: (i) improved statistical methods (e.g. ridge regression, correlation coefficient filtering) as proposed in those works. (ii) Direct 4D parametric imaging which already investigated for this particular problem to some extent [104, 105].

(b) It may be stated that initial 6min PET scan for the purpose of input function estimation is not appropriate use of resources. Furthermore, early PET imaging (<<60min post-injection) has the additional disadvantage that conventional SUV images cannot be generated. It may be instead meaningful to scan at later stages (e.g. 45-75min or 60-90min post-injection), where a population input function is used, but this time scaled using multiple late-phase input function estimates (by subsequent passes over the heart), which at the same time enables generation of SUV-type images by simple summation of the frames. This can then be utilized to enable complementary generation of SUV and parametric images for enhanced clinical and quantitative task performance, and clinicians can be provided with both views.

Finally, we note that the abovementioned overall framework may also be promising in non-oncology applications. In particular, parametric imaging of blood vessels has to potential to enhance visualization and quantification of the atherosclerotic burden. This is because, similar to what black-blood MRI pursues [106], this approach may enable saturation of the signal at the center of the vessel lumen while focal uptake at the periphery of the vessel walls can be detected [107].

1.6.3   4-D kinetic parameter estimation strategies

To maintain the intrinsic spatial resolution characteristics provided by the current PET systems, kinetic parameter estimation can be performed at the voxel level providing parametric images of physiologically and biologically related parameters. However as kinetic modelling is performed at each voxel, the resulting TACs can be substantially noisier compared to regional TACs. This problem has long been identified and has restricted the widespread use of parametric imaging in clinical practice, as parametric maps can be very noisy, reducing their potential value in different clinical applications. Originally the problem associated with deriving noisy parametric maps stems from the two-step approach traditionally used in estimating kinetic parameters, with independently reconstructed time frames followed by kinetic modelling. To tackle the problem one can incorporate temporal information after or during reconstruction, imposing constrains and resulting in less biased and more precise parameter estimates. A differentiation can be made, as some of these methods make use of a non-physiologically based temporal model, as a means of temporal regularization prior to parameter estimation. These methods are referred to as 'indirect' 4-D methods, as although they use a model as a temporal constraint between the frames, they deliver parameter estimates via a 2 step route. In a second group of methods, a joint approach to parameter estimation is used, where kinetic parameters are estimated directly during or before the reconstruction process, in a single step. These methods are often referred to as 'direct' 4-D methods as they use physiologically meaningful kinetic models. As such, the task of image reconstruction can be thought as of reconstructing parameter estimates directly from measured projections, without any intermediate step [108-110].

1.6.3.1 Indirect parameter estimation using temporal regularization

Temporal smoothing is based on the similar behaviour neighbouring time frames have. Walledge et al [111] exploiting this concept, applied a filtered image of the previous frame as the initializing image for the next frame. Temporal smoothing has also been used within a MAP framework [112-116] while Reader et al [117] interchanged the reconstructed intensity between iterations with the fitted images, omitting the need for any prior term.

   Another way to tackle the SNR problem is to consider temporal basis functions (TBF) representing a wide range of possible kinetics in the data. The use of TBF is based either on the data itself or the physiologic model under study. In the former case a smoothing is achieved while in the latter, the basis coefficients have physiologic meaning. Using b-spline TBF, Asma et al [118] and Nichols et al [119] reconstructed a set of basis function coefficients having though no physiological meaning. Nichols et al [119] used information from the head curve to optimize the splines, while Verhaeghe et al [120] used the inter-iterations TACs. In an extension of the method, Verhaeghe et al [121-123] proposed joint estimation of coefficients and b-spline TBF. This approach has similarities to the method of Reader et al [124, 125] where the TBF are not specified a priori but are left to be jointly estimated with the coefficients in an interleaving fashion.

   Similar temporal smoothing can be achieved using wavelets decomposition [126-128]. This decomposition gives a set of coefficients for a set of basis functions. By thresholding the coefficients, a signal denoising is achieved. Turkheimer et al [129] pioneered the field by applying kinetic modelling in the wavelet space while Verhaeghe et al [130] used a spatiotemporal wavelet basis function within a fully 4-D reconstruction.
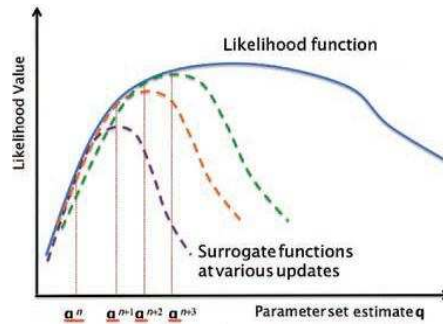
Fig 6. Optimization using surrogate functions that are iteratively constructed and maximized providing subsequent updates [131].

1.6.3.2 Direct parameter estimation strategies

All the aforementioned methods are trying to improve SNR, without though considering the kinetic parameter estimation problem, which is the endpoint of image reconstruction in dynamic imaging. In order to simplify the parameter estimation sequence and directly reconstruct parameters of interest in a single step, a joint approach can be used to create parametric images by modelling the data before or during reconstruction.

1.6.3.2.1   Reconstructing parametric sinograms

One approach is to apply the kinetic modelling directly on the projection data, so as to reconstruct a single set of parametric sinograms [132-134]. Spectral analysis of the projection data has been used by Matthews et al [135] and Meikle et al [136]. This modelling approach is particularly advantageous in oncology, where the in vivo radiotracer distribution is not known for new anticancerous drugs. The method provided improved SNR compared to the conventional approach, but with expense of bias. This was attributed to the noisy data and the fact that the projection data contain heterogeneous dynamics from different tissues along a given LOR, causing adjacent coefficients to merge. Patlak analysis has also been used on wevelet transformed projections, resulting in 2 macro-parameter images [137]. Although direct sinogram methods result in reconstructing parametric images, they can only be applied with linear models which can be extended to projection space, as the projections are linearly related with the pixels along a given LOR. Also after modelling the data the Poisson distribution is no longer a valid assumption.

1.6.3.2.2   Spatiotemporal 4-D image reconstruction

A problem encountered in post-reconstruction kinetic modelling is the accurate knowledge of the noise distribution in every reconstructed frame, in order to weight the data contribution during the fitting procedure. While analytic and approximate formulae for the weighting can be calculated for FBP reconstructed data, in iterative reconstruction methods, such a formula is not straightforward. This is due to pixel correlations and algorithm non-linearity, with the noise being object specific and vary within the reconstructed FOV. Incorporating the kinetic parameter estimation within image reconstruction results in a more accurate modelling of the noise propagation from Poisson distributed raw projection data to the kinetic parameters.

Direct reconstruction of regional kinetics have been used in the past [138-141], however ROI approaches suffers from all the aforementioned problems mentioned previously. As such,

direct parametric imaging is the obvious way to calculate parameters, while preserving spatial resolution. It was Snyder et al [142] and Carson and Lange [143] who first proposed such a scheme within an EM algorithm, without though implementing it. A plethora of direct parametric reconstruction methods have been implemented since then, both for linear and non-linear kinetic models.

Linear models

Wang et al [144] incorporated a Patlak graphical analysis model with a MAP reconstruction, while Tsoumpas et al [109] used Patlak analysis along with the parametric iterative reconstruction algorithm of Matthews et al [135], showing improved SNR and mean square error (MSE). Similar modelling has been used to directly estimate patlak parameter from list mode data [145]. Tang et al [146] proposed a similar closed form algorithm, incorporating anatomical information from MR and using the joint entropy between the MR and PET parametric features as a prior, while Rahmim et al [147] applied a 4-D algorithm for direct Patlak parameter estimation in oncology FDG patients, showing reduced noise compared to conventional Patlak parametric images. Merlin et al [148] advanced the field further by incorporating a motion correction scheme within a Patlak 4-D reconstruction using the NCAT phantom. Finally Rahmim et al [149] developed and applied a direct AB-EM image reconstruction using the relative equilibrium graphical analysis formulation for reversibly binding tracers, exhibiting ~35% noise reduction in DV and DVR parameters compared to post-reconstruction methods.

Apart from graphical analysis models, data driven models have also been used within a 4-D framework. Reader et al [150] advanced the field by simultaneously estimating a system IF and the spectral coefficients. In a first step, the coefficients are optimized keeping the IF constant, while in a second step the coefficients are kept constant optimizing the IF. The method has been used by the authors as a means to regularize the data and as such it belongs to the TBF approaches. In the case of a true IF though, it can return the true BF coefficients and in this sense is a direct method. Wang and Qi [151] used a similar approach to include spectral analysis within a MAP reconstruction, using a Laplacian prior as sparsity constraint, similar to the one used by Gunn et al [152] in the basis pursuit approach to spectral analysis.

Non-linear models

4-D reconstruction algorithms based on linear kinetic models can deliver direct estimates of macro-parameter images. Such estimates are more robust to noise and potentially easier to estimate and interpret with a clinical environment. However further information are available from full compartmental analysis based on non-linear model, with respect to constant rate between the different physiologic compartments. Kamasak et al [153] was one of the first to directly derive a set of micro-parameters of interest, using the 2-tissue compartmental model with a MAP criterion and a coordinate descent algorithm. Since the model is nonlinear in its parameters, the algorithm has nested optimization sub-algorithms to decouple the non-linearity from the system model. EM [154] and PCG [155] based direct reconstruction algorithm have also been used for the 1-tissue compartment model .

Decoupling the spatiotemporal image reconstruction problem

Deriving micro-parameter maps from noisy dynamic data can result in biased and noisy parametric images which in turn is a major stumbling block in their widespread application in
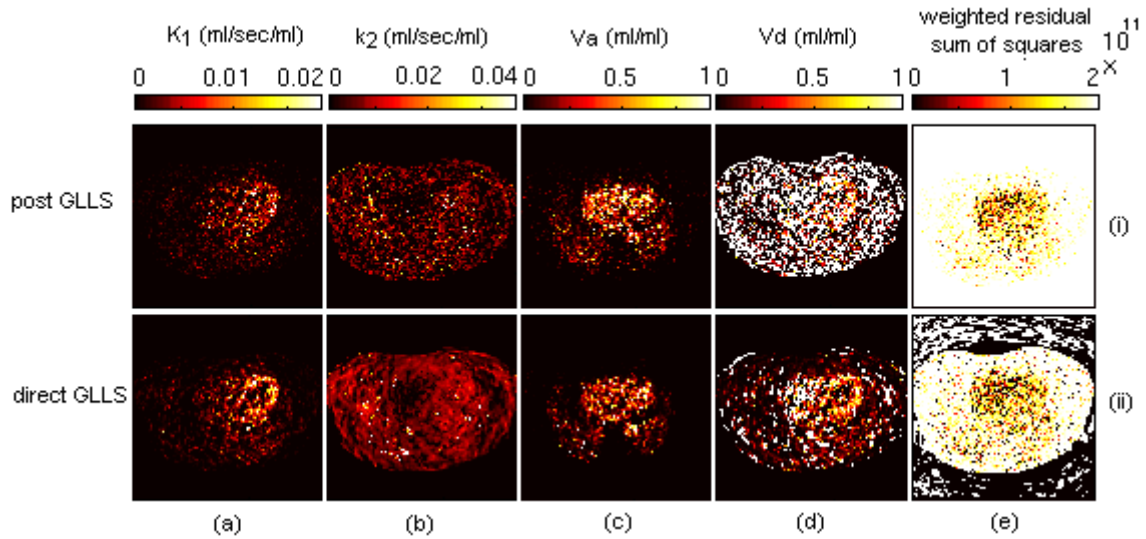
Fig 7. Parametric images of perfusion (K_1) (a), efflux rate (k_2) (b), fractional blood volume (V_a) (c), volume of distribution (V_d) (d) and weighted residual sum of squares (e) calculated from dynamic thoracic $[^{15}O]H_2O$ PET data with post-reconstruction kinetic analysis and direct 4-D image reconstruction. Good separation of the tissue constant rates and blood volume is seen with the direct method improving variance in kinetic parameter [156].

clinical practice as already mentioned. However the aforementioned direct 4-D image reconstruction approaches have been shown time and time again to improve both accuracy and precision in the kinetic parameters compared to their post-reconstruction counterparts with the degree of improvement varying depending on the injected tracer and the kinetic model used. Nevertheless despite the improved bias and variance in micro-parameter maps, 4-D algorithms incorporating nonlinear compartmental models are time consuming, complex and usually slow to converge, rendering them difficult to be applied in clinical practice. These algorithms are also restricted to a specific combination of spatial and temporal models. These issues stem from the coupling between the tomographic image reconstruction problem and the kinetic parameter estimation problem. In order to avoid optimising the 4D log-likelihood function a convenient method is to transfer the optimization problem to surrogate functions which are more easily optimized (Fig. 6). To tackle these issues Wang and Qi [157] proposed an algorithm to decouple these 2 components using this optimization transfer principle and paraboloidal surrogate functions. In an extension of this work, they used linear Patlak and spectral analysis models as well as nonlinear models within a nested EM algorithm [158, 159]. Similar is the work of Matthews et al [160] in which following separation between the image and projection space problems, the ML image based problem is transformed into a LS problem for which many existing methods can be used. The method has been implemented with 1-tissue (Fig. 7) [156], irreversible 2-tissue (Fig. 8) [161, 162] and reversible simplified reference tissue [163] models, in perfusion, metabolism and neureceptor imaging studies respectively, with improved parameter precision and accuracy compared to post-reconstruction kinetic modelling approaches. Using the same optimization transfer approach also Wang and Qi [164] developed a minorization-maximization algorithm to include a simplified reference tissue model within a 4-D framework. Finally, along similar lines with the work of Wang and Qi [157, 158] and Matthews et al [160] is the work of Rahmim et al [131], who also used a decoupling technique and a surrogate function with a single compartment model to directly estimate myocardial perfusion in ^{82}Rb imaging. Achieving a decoupling between the tomographic and the image based kinetic modelling problem has facilitated the use of existing image reconstruction and kinetic modelling algorithms in a way similar to the post-reconstruction modelling approach but monotonically converging to the direct parameter estimates. This in turn allows the direct estimation of micro-parameter
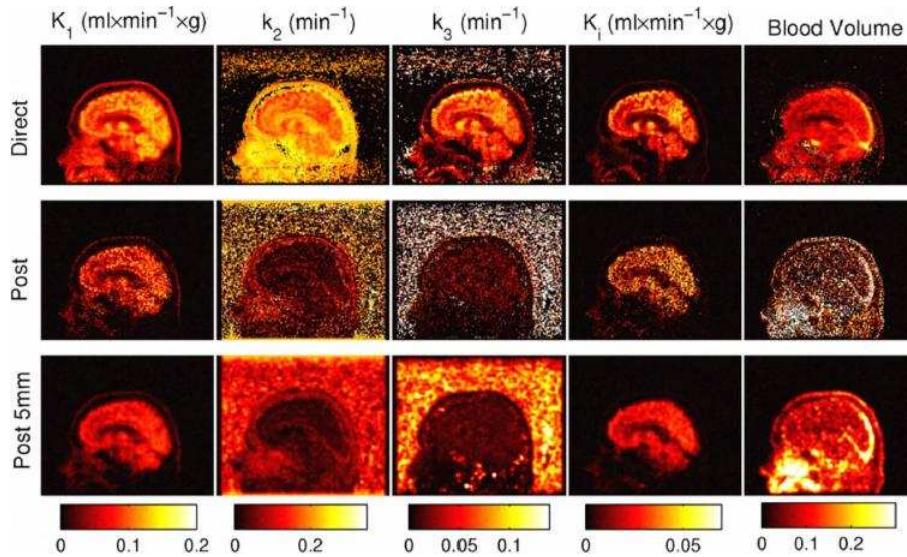
Fig 8. Parametric maps from dynamic brain [^{18}F]FDG PET data calculated with direct 4-D image reconstruction (top row) using optimization transfer and the conventional post-reconstruction method (middle row), along with its post-filtered version with a 5mm Gaussian kernel (bottom row) at the 12th tomographic iteration [162].

images in a fast and efficient manner, with faster convergence, while at the same time achieving improved precision and accuracy compared to post-reconstruction kinetic analysis, making their clinical implementation and application a more feasible task. Despite the improvements offered by 4-D reconstruction algorithms however, their application in the body can be complicated by the various kinetics encountered within the FOV. Using a common simple kinetic model within a 4-D reconstruction framework may lead to bias from erroneously modelled regions, propagate to other regions for which the model is accurate [165]. To prevent this bias propagation, Matthews et al [166] proposed an adaptive kinetic model algorithm to be incorporated within a 4-D reconstruction [167]. The algorithm introduces a secondary less constrained model which is adaptively included for voxels that the primary model in not able to fit An analytic derivation of the different direct parameter estimation schemes has been reported by Wang and Qi [110].

1.6.4 Synergistic benefits of PET/MR imaging in pharmacokinetic modelling

PET and MR can provide complementary anatomical and functional information of the system under study. Synergistic benefits can also be pooled by fusing the images using either co-registration techniques or sequential PET/MR imaging between the 2 modalities [168, 169]. However with the advent of simultaneous PET/MR systems and the resulting spatiotemporal correlation of the respective data, additional information can become available, further enhancing the capabilities of these bimodal systems [170]. Although PET/CT is an established modality in oncology, as well as neurology and cardiology, the clinical importance of PET/MR is yet to be fully exploited, with limited applications showing its superiority against PET/CT and limiting is clinical importance. However simultaneous PET/MR has potentially the advantage to open the road to the clinical application of dynamic imaging and pharmacokinetic modelling protocols.

As elaborated previously, one of the main obstacles in the clinical adoption of kinetic analysis studies is the importance and necessity of an accurate estimation of the input function. AIFs are the gold standard but IDIFs present a more feasible alternative in the clinic, owing to the difficulties with arterial catheterization. However extraction of IDIFs require accurate localization of the vasculature which not always possible using CT data, especially in
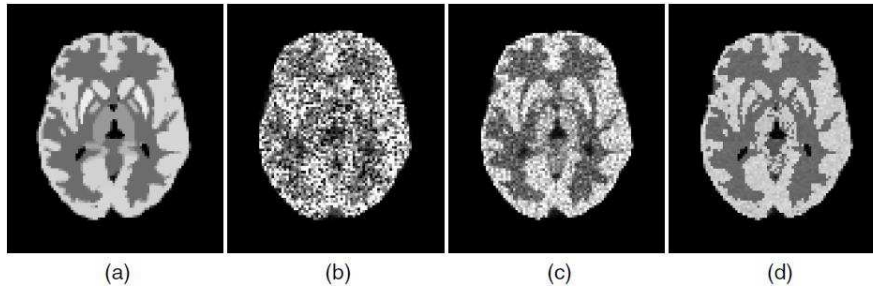
Fig 9. Transaxial slice of the Patlak slope image of (a) the phantom image, (b) the image estimated from 3D reconstruction followed by modeling (the second iteration), (c) the direct 4D parametric reconstruction (the fifth iteration) and (d) the 4D direct MAP parametric reconstruction incorporating the MR image information (the fifth iteration) [146].

neuroimaging studies. Furthermore registration accuracy provided between separate PET and MR datasets at different physiologic states or even in sequential PET/MR imaging, might not be sufficient when small vessels, such as the small carotic artery, need to be delineated [71]. Simultaneous acquisition of the respective structural and anatomical information ensures accurate registration between the 2 datasets and precise localization of the ROI to be delineated. Nevertheless accurate delineation is only one of the problems associated with IDIF and spill-in and spill-out effects are also a major concern. However again simultaneously acquired MR data can be used within an MR-guided PET image reconstruction, with anatomical information acting as priors within a MAP framework [171-175] or using them for IF correction based on estimating recovery coefficients [73]. Inclusion of MR prior information can also be extended to direct 4-D image reconstruction (Fig. 9) for improved variance in the kinetic parameters [176]. This synergistic benefit between the 2 modalities goes beyond the IDIF correction and can assist in assessing cancerous regions with heterogeneous kinetics. Partial volume effects in these regions usually result in adjacent kinetics, especially at the boundaries of tissues with differential physiology, being averaged. MR-based PVC methods in simultaneous PET/MR can help particularly in treatment response or drug efficacy studies by assessing potentially heterogeneous kinetics within the target region.

Another area that simultaneously MR data can assist dynamic imaging protocols is motion correction [177-182]. In kinetic analysis dynamic studies, motion occurs both within each temporal frame due to respiration, cardiac contraction and involuntary patient movement as well as across temporal frames again due to involuntary patient movement. Both inter- and intra-frame motion causes adjacent kinetics to be averaged resulting in erroneous TACs and subsequently in erroneous kinetic parameters. Furthermore attenuation-emission mismatches causes further degradation in the parameter estimates. Motion tracking with various external optical sensors has been used in dynamic imaging protocols with varying accuracy due to difficulties associated both with hardware and software complexity. Furthermore such techniques are inefficient in PET/MR due to the coils preventing the optical sensors from having a clear FOV. However using high temporal resolution MR data acquired during the dynamic PET acquisition, the motion vectors can be estimated providing motion correction both within as well as across frames. The temporal resolution is offered by the MR system is of particular importance in the early time frames where short frames are acquired to capture the fast influx phase of the tracer's distribution. Apart from the potential of improving the kinetics parameters through MR-derived motion correction, the IDIF calculation can also benefit from such motion correction schemes [183]. Recent advancement are summarized in review of MR-based motion correction schemes [184].

Apart from improvements on the PET data, MR information can be used to facilitate more reliable kinetic parameters during parameter estimation. Fluckiger et al [185] used DCE-MRI

17
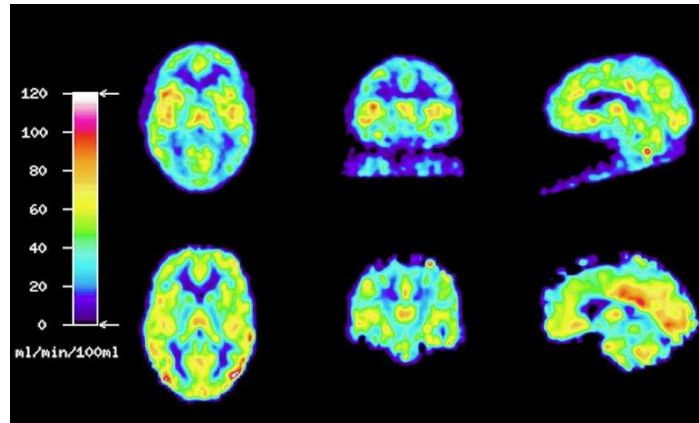
Fig 10. Comparison of parametric images of cerebral blood flow (CBF) obtained in the hybrid 3 T MR–PET scanner. PET CBF images (top) were obtained simultaneously with MRI CBF images (bottom) ASL. Arterial input function was obtained by continuous blood sampling from the radial artery using an MR-compatible blood monitor and corrected for delay and dispersion [186].

data to separate the blood volume component from the whole tissue TAC enabling kinetic parameter estimation with fewer free parameters while Poulin et al interchanged input functions estimated with PET and MR [187].

Methodological synergies between the 2 modalities is not the only incentive in simultaneous dynamic PET/MR imaging, as application synergies are also possible. Dynamic imaging with $[^{15}O]H_2O$ and $^{15}O_2$ is used to assess perfusion and metabolic rate of oxygen as well as oxygen extraction and to date these parameters are mainly used for assessing anti-angiogenesis drug efficacy after neo-adjuvant of primary chemotherapy, tumor brain imaging, myocardium imaging, as well as activation studies. However similar haemodynamic parameters can be estimated from a variety of MR techniques, such arterial spin labelling and DCE-MRI, and fMRI. Comparison of blood flow estimates from individual PET and MR studies have been reported [188, 189]. However performing haemodynamic measurements in dynamic PET/MR could provide parameters estimated simultaneously from each respective modality as shown in Fig. 10 and compared to each other for cross-validation [186] [190]. Additionally complementary information provided by the PET and the MR can also be used to assess their functional relationship. Apart from oncology and neuroimaging, cardiology could also benefit from simultaneous dynamic PET/MR myocardial perfusion studies with ^{82}Rb. Limited studies have been reported so far on the application of dynamic PET/MR in pharmacokinetic modelling. However due the aforementioned benefits of MR, more research groups are steering their efforts towards methodological development and clinical applications in simultaneous dynamic PET/MR imaging.

1.7 Conclusion

In this note we tried to give an overview of the recent advancements in kinetic modelling which could facilitate their routine use in clinical practice. Throughout this work emphasis was given in oncology $[^{18}F]$FDG PET imaging due its extensive utilization in clinical practice. We realize that some of the reviewed methods and techniques are potentially only applicable in a research environment due to their complexity. However we expect that the aforementioned advancements in input function estimation, coupled to improvements in acquisition protocol design and parameter estimation algorithms could make dynamic imaging a feasible alternative to static imaging with fully quantitative parameters based on

kinetic modelling complementing or even superseding semi-quantitative analysis in the clinic. Whole-body parametric imaging has already been proven to be a applicable in a clinical environment while direct 4-D image reconstruction methods have demonstrated superior precision and accuracy in kinetic parameter estimation. Extending these techniques to PET/MR imaging could potentially revolutionize the way clinical imaging is performed, enhancing the potentials of PET/MR and extending its application and scope to dynamic multi-parametric imaging in the clinic.

Acknowledgements

[1]   A. Buerkle and W. A. Weber, "Imaging of tumor glucose utilization with positron emission tomography.," Cancer Metastasis Rev, vol. 27, pp. 545-554, Dec 2008.

[2]   K. R. Zasadny and R. L. Wahl, "Standardized uptake values of normal tissues at PET with 2-[fluorine-18]-fluoro-2-deoxy-D-glucose: variations with body weight and a method for correction," Radiology, vol. 189, pp. 847-850, 1993.

[3]   C. K. Kim, N. C. Gupta, B. Chandramouli, and A. Alavi, "Standardized uptake values of FDG: body surface area correction is preferable to body weight correction," J Nucl Med, vol. 35, pp. 164-167, 1994.

[4]   C. K. Kim and N. C. Gupta, "Dependency of standardized uptake values of fluorine-18 fluorodeoxyglucose on body size: comparison of body surface area correction and lean body mass correction," Nucl Med Commun., vol. 17, pp. 890-894, 1996.

[5]   R. L. Wahl and J. W. Buchanan, Principles and Practice of Positron Emission Tomography vol. 1st. Philadelphia, PA: Lippincott Williams & Wilkins, 2002.

[6]   N. Sadato, T. Tsuchida, S. Nakaumra, A. Waki, H. Uematsu, N. Takahashi, et al., "Non-invasive estimation of the net influx constant using the standardized uptake value for quantification of FDG uptake of tumours," Eur.J Nucl Med, vol. 25, pp. 559-564, 1998.

[7]   L. M. Hamberg, G. J. Hunter, N. M. Alpert, N. C. Choi, J. W. Babich, and A. J. Fischman, "The Dose Uptake Ratio as an Index of Glucose Metabolism: Useful Parameter or Oversimplification?," J Nucl Med, vol. 35, pp. 1308-1312, August 1, 1994 1994.

[8]   J. W. Keyes, Jr., "SUV: Standard Uptake or Silly Useless Value?," J Nucl Med, vol. 36, pp. 1836-1839, October 1, 1995 1995.

[9]   H. Sung-Cheng, "Anatomy of SUV," Nuclear medicine and biology, vol. 27, pp. 643-646, 2000.

[10]   M. C. Adams, T. G. Turkington, J. M. Wilson, and T. Z. Wong, "A systematic review of the factors affecting accuracy of SUV measurements," AJR Am.J Roentgenol., vol. 195, pp. 310-320, 2010.

[11]   P. Cheebsumon, L. M. Velasquez, C. J. Hoekstra, W. Hayes, R. W. Kloet, N. J. Hoetjes, et al., "Measuring response to therapy using FDG PET: semi-quantitative and full kinetic analysis," Eur J Nucl Med Mol Imaging, vol. 38, pp. 832-42, May 2011.

[12]   M. Allen-Auerbach and W. A. Weber, "Measuring Response with FDG-PET: Methodological Aspects," Oncologist, vol. 14, pp. 369-377, April 1, 2009 2009.

[13]   Y. Sugawara, K. R. Zasadny, H. B. Grossman, I. R. Francis, M. F. Clarke, and R. L. Wahl, "Germ cell tumor: differentiation of viable tumor, mature teratoma, and necrotic

tissue with FDG PET and kinetic modeling," Radiology, vol. 211, pp. 249-56, Apr 1999.

[14] W. A. Weber, S. I. Ziegler, R. Thodtmann, A.-R. Hanauske, and M. Schwaiger, "Reproducibility of Metabolic Measurements in Malignant Tumors Using FDG PET," J Nucl Med, vol. 40, pp. 1771-1777, November 1, 1999 1999.

[15] S. Leskinen-Kallio, K. Nagren, P. Lehikoinen, U. Ruotsalainen, M. Teras, and H. Joensuu, "Carbon-11-Methionine and PET Is an Effective Method To Image Head and Neck Cancer," J Nucl Med, vol. 33, pp. 691-695, May 1, 1992 1992.

[16] S. C. Huang, "Anatomy of SUV. Standardized uptake value," Nucl Med Biol, vol. 27, pp. 643-6, Oct 2000.

[17] R. Boellaard, "Standards for PET image acquisition and quantitative data analysis.," J Nucl Med, vol. 50, pp. 11S-20, May 1, 2009 2009.

[18] M. C. Adams, T. G. Turkington, J. M. Wilson, and T. Z. Wong, "A systematic review of the factors affecting accuracy of SUV measurements.," AJR Am J Roentgenol, vol. 195, pp. 310-320, Aug 2010.

[19] P. D. Shreve, Y. Anzai, and R. L. Wahl, "Pitfalls in Oncologic Diagnosis with FDG PET Imaging: Physiologic and Benign Variants," Radiographics, vol. 19, pp. 61-77, 1999.

[20] L. G. Strauss, "Fluorine-18 deoxyglucose and false-positive results: a major problem in the diagnostics of oncological patients," European journal of nuclear medicine and molecular imaging, vol. 23, pp. 1409-1415, 1996.

[21] M. A. Lodge, J. D. Lucas, P. K. Marsden, B. F. Cronin, M. J. O'Doherty, and M. A. Smith, "A PET study of 18FDG uptake in soft tissue masses," European journal of nuclear medicine and molecular imaging, vol. 26, pp. 22-30, 1999.

[22] O. Schillaci, L. Travascio, F. Bolacchi, F. Calabria, C. Bruni, C. Ciccio, et al., "Accuracy of early and delayed FDG PET-CT and of contrast-enhanced CT in the evaluation of lung nodules: a preliminary study on 30 patients," Radiol.Med, vol. 114, pp. 890-906, 2009.

[23] Y. Umeda, Y. Demura, T. Ishizaki, S. Ameshima, I. Miyamori, Y. Saito, et al., "Dual-time-point 18F-FDG PET imaging for diagnosis of disease type and disease activity in patients with idiopathic interstitial pneumonia," Eur.J Nucl Med Mol.Imaging, vol. 36, pp. 1121-1130, 2009.

[24] S. Sanz-Viedma, D. A. Torigian, M. Parsons, S. Basu, and A. Alavi, "Potential clinical utility of dual time point FDG-PET for distinguishing benign from malignant lesions: implications for oncological imaging," Rev.Esp.Med Nucl, vol. 28, pp. 159-166, 2009.

[25] Y. Yamamoto, R. Kameyama, T. Togami, N. Kimura, S. Ishikawa, and Y. Nishiyama, "Dual time point FDG PET for evaluation of malignant pleural mesothelioma," Nucl Med Commun., vol. 30, pp. 25-29, 2009.

[26] Y. Nishiyama, Y. Yamamoto, N. Kimura, S. Ishikawa, Y. Sasakawa, and M. Ohkawa, "Dual-time-point FDG-PET for evaluation of lymph node metastasis in patients with non-small-cell lung cancer," Ann.Nucl Med, vol. 22, pp. 245-250, 2008.

[27] X. L. Lan, Y. X. Zhang, Z. J. Wu, Q. Jia, H. Wei, and Z. R. Gao, "The value of dual time point (18)F-FDG PET imaging for the differentiation between malignant and benign lesions," Clin.Radiol., vol. 63, pp. 756-764, 2008.

[28] P. Liu, G. Huang, S. Dong, and L. Wan, "Kinetic analysis of experimental rabbit tumour and inflammation model with 18F-FDG PET/CT," Nuklearmedizin, vol. 48, pp. 153-158, 2009.

[29] M. Houseni, W. Chamroonrat, J. Zhuang, R. Gopal, A. Alavi, and H. Zhuang, "Prognostic implication of dual-phase PET in adenocarcinoma of the lung," J Nucl Med, vol. 51, pp. 535-542, 2010.

[30] Y. Xiu, C. Bhutani, T. Dhurairaj, J. Q. Yu, S. Dadparvar, S. Reddy, et al., "Dual-time point FDG PET imaging in the evaluation of pulmonary nodules with minimally increased metabolic activity," Clin.Nucl Med, vol. 32, pp. 101-105, 2007.

[31] D. Uesaka, Y. Demura, T. Ishizaki, S. Ameshima, I. Miyamori, M. Sasaki, et al., "Evaluation of dual-time-point 18F-FDG PET for staging in patients with lung cancer," J Nucl Med, vol. 49, pp. 1606-1612, 2008.

[32] R. Hustinx, R. J. Smith, F. Benard, D. I. Rosenthal, M. Machtay, L. A. Farber, et al., "Dual time point fluorine-18 fluorodeoxyglucose positron emission tomography: a potential method to differentiate malignancy from inflammation and normal tissue in the head and neck," Eur.J Nucl Med, vol. 26, pp. 1345-1348, 1999.

[33] A. Matthies, M. Hickeson, A. Cuchiara, and A. Alavi, "Dual time point 18F-FDG PET for the evaluation of pulmonary nodules," J Nucl Med, vol. 43, pp. 871-875, 2002.

[34] R. Kumar, V. A. Loving, A. Chauhan, H. Zhuang, S. Mitchell, and A. Alavi, "Potential of dual-time-point imaging to improve breast cancer diagnosis with (18)F-FDG PET," J Nucl Med, vol. 46, pp. 1819-1824, 2005.

[35] Y. Nishiyama, Y. Yamamoto, K. Fukunaga, N. Kimura, A. Miki, Y. Sasakawa, et al., "Dual-time-point 18F-FDG PET for the evaluation of gallbladder carcinoma," J Nucl Med, vol. 47, pp. 633-638, 2006.

[36] S. Y. Ma, L. C. See, C. H. Lai, H. H. Chou, C. S. Tsai, K. K. Ng, et al., "Delayed (18)F-FDG PET for detection of paraaortic lymph node metastases in cervical cancer patients," J Nucl Med, vol. 44, pp. 1775-1783, 2003.

[37] A. M. Spence, M. Muzi, D. A. Mankoff, S. F. O'Sullivan, J. M. Link, T. K. Lewellen, et al., "18F-FDG PET of gliomas at delayed intervals: improved distinction between tumor and normal gray matter," J Nucl Med, vol. 45, pp. 1653-9, Oct 2004.

[38] S. Sanz-Viedma, D. RTorigian, M. Parsons, S. Basu, and A. Alavi, "Potential clinical utility of dual time point FDG-PET for distinguishing benign from malignant lesions: implications for oncological imaging," Rev Esp Med Nucl, vol. 28, pp. 159-66, 2009.

[39] H. Zhuang, M. Pourdehnad, E. S. Lambright, A. J. Yamamoto, M. Lanuti, P. Li, et al., "Dual time point 18F-FDG PET imaging for differentiating malignant from inflammatory processes," J Nucl Med, vol. 42, pp. 1412-1417, 2001.

[40] M. Houseni, W. Chamroonrat, J. Zhuang, R. Gopal, A. Alavi, and H. Zhuang, "Prognostic Implication of Dual-Phase PET in Adenocarcinoma of the Lung," J Nucl Med, p. jnumed.109.068643, March 17, 2010 2010.

[41] Freedman, N. M. T., Sundaram, S. K., Kurdziel, Karen, et al., "Comparison of SUV and Patlak slope for monitoring of cancer therapy using serial PET scans," European journal of nuclear medicine and molecular imaging, vol. 30, p. 8, 2003.

[42] K. Ishizu, S. Nishizawa, Y. Yonekura, N. Sadato, Y. Magata, N. Tamaki, et al., "Effects of Hyperglycemia on FDG Uptake in Human Brain and Glioma," J Nucl Med, vol. 35, pp. 1104-1109, July 1, 1994 1994.

[43] J. A. Thie, "Clarification of a Fractional Uptake Concept," J Nucl Med, vol. 36, pp. 711-b-712, April 1, 1995 1995.

[44] G. J. Hunter, L. M. Hamberg, N. M. Alpert, N. C. Choi, and A. J. Fischman, "Simplified measurement of deoxyglucose utilization rate," J Nucl Med, vol. 37, pp. 950-5, Jun 1996.

[45] P. Cheebsumon, L. M. Velasquez, C. J. Hoekstra, W. Hayes, R. W. Kloet, N. J. Hoetjes, et al., "Measuring response to therapy using FDG PET: semi-quantitative and full kinetic analysis.," Eur J Nucl Med Mol Imaging, vol. 38, pp. 832-842, May 2011.

[46] M. M. Graham, L. M. Peterson, and R. M. Hayward, "Comparison of simplified quantitative analyses of FDG uptake," Nucl Med Biol, vol. 27, pp. 647-55, Oct 2000.

[47] C. J. Hoekstra, I. Paglianiti, O. S. Hoekstra, E. F. Smit, P. E. Postmus, G. J. Teule, et al., "Monitoring response to therapy in cancer using [18F]-2-fluoro-2-deoxy-D-

glucose and positron emission tomography: an overview of different analytical methods," Eur J Nucl Med, vol. 27, pp. 731-43, Jun 2000.

[48]   C. J. Hoekstra, O. S. Hoekstra, S. G. Stroobants, J. Vansteenkiste, J. Nuyts, E. F. Smit, et al., "Methods to monitor response to chemotherapy in non-small cell lung cancer with 18F-FDG PET," J Nucl Med, vol. 43, pp. 1304-9, Oct 2002.

[49]   A. A. Lammertsma, C. J. Hoekstra, G. Giaccone, and O. S. Hoekstra, "How should we analyse FDG PET studies for monitoring tumour response?," Eur J Nucl Med Mol Imaging, vol. 33 Suppl 1, pp. 16-21, Jul 2006.

[50]   Y. Nishiyama, Y. Yamamoto, T. Monden, Y. Sasakawa, N. Kawai, K. Satoh, et al., "Diagnostic value of kinetic analysis using dynamic FDG PET in immunocompetent patients with primary CNS lymphoma," Eur J Nucl Med Mol Imaging, vol. 34, pp. 78-86, Jan 2007.

[51]   Y. Nishiyama, Y. Yamamoto, T. Monden, Y. Sasakawa, N. Kawai, K. Satoh, et al., "Diagnostic value of kinetic analysis using dynamic FDG PET in immunocompetent patients with primary CNS lymphoma.," Eur J Nucl Med Mol Imaging, vol. 34, pp. 78-86, Jan 2007.

[52]   N. Kawai, Y. Nishiyama, K. Miyake, T. Tamiya, and S. Nagao, "Evaluation of tumor FDG transport and metabolism in primary central nervous system lymphoma using [18F]fluorodeoxyglucose (FDG) positron emission tomography (PET) kinetic analysis," Ann Nucl Med, vol. 19, pp. 685-90, Dec 2005.

[53]   Y. Anzai, S. Minoshima, G. T. Wolf, and R. L. Wahl, "Head and neck cancer: detection of recurrence with three-dimensional principal components analysis at dynamic FDG PET," Radiology, vol. 212, pp. 285-90, Jul 1999.

[54]   C. Schiepers, W. Chen, T. Cloughesy, M. Dahlbom, and S. C. Huang, "18F-FDOPA kinetics in brain tumors," J Nucl Med, vol. 48, pp. 1651-61, Oct 2007.

[55]   D. Thorwarth, S. M. Eschmann, F. Paulsen, and M. Alber, "A kinetic model for dynamic [18F]-Fmiso PET data to analyse tumour hypoxia.," Phys Med Biol, vol. 50, pp. 2209-2224, May 21 2005.

[56]   C. Schiepers, W. Chen, M. Dahlbom, T. Cloughesy, C. K. Hoh, and S. C. Huang, "18F-fluorothymidine kinetics of malignant brain tumors," Eur J Nucl Med Mol Imaging, vol. 34, pp. 1003-11, Jul 2007.

[57]   M. Wardak, C. Schiepers, M. Dahlbom, T. Cloughesy, W. Chen, N. Satyamurthy, et al., "Discriminant analysis of (1)(8)F-fluorothymidine kinetic parameters to predict survival in patients with recurrent high-grade glioma," Clin Cancer Res, vol. 17, pp. 6553-62, Oct 15 2011.

[58]   T. Tsuchida, Y. Demura, M. Sasaki, M. Morikawa, Y. Umeda, T. Tsujikawa, et al., "Differentiation of histological subtypes in lung cancer with 18F-FDG-PET 3-point imaging and kinetic analysis," Hell J Nucl Med, vol. 14, pp. 224-7, Sep-Dec 2011.

[59]   L. G. Strauss, S. Klippel, L. Pan, K. Schonleben, U. Haberkorn, and A. Dimitrakopoulou-Strauss, "Assessment of quantitative FDG PET data in primary colorectal tumours: which parameters are important with respect to tumour detection?," Eur J Nucl Med Mol Imaging, vol. 34, pp. 868-77, Jun 2007.

[60]   L. G. Strauss, D. Koczan, S. Klippel, L. Pan, C. Cheng, S. Willis, et al., "Impact of angiogenesis-related gene expression on the tracer kinetics of 18F-FDG in colorectal tumors," J Nucl Med, vol. 49, pp. 1238-44, Aug 2008.

[61]   L. G. Strauss, D. Koczan, S. Klippel, L. Pan, C. Cheng, U. Haberkorn, et al., "Impact of cell-proliferation-associated gene expression on 2-deoxy-2-[(18)f]fluoro-D-glucose (FDG) kinetics as measured by dynamic positron emission tomography (dPET) in colorectal tumors," Mol Imaging Biol, vol. 13, pp. 1290-300, Dec 2011.

[62]   A. Dimitrakopoulou-Strauss, L. G. Strauss, C. Burger, A. Ruhl, G. Irngartinger, W. Stremmel, et al., "Prognostic aspects of 18F-FDG PET kinetics in patients with

metastatic colorectal carcinoma receiving FOLFOX chemotherapy," J Nucl Med, vol. 45, pp. 1480-7, Sep 2004.

[63]   A. Dimitrakopoulou-Strauss, L. G. Strauss, M. Schwarzbach, C. Burger, T. Heichel, F. Willeke, et al., "Dynamic PET 18F-FDG studies in patients with primary and recurrent soft-tissue sarcomas: impact on diagnosis and correlation with grading," J Nucl Med, vol. 42, pp. 713-20, May 2001.

[64]   S. Okazumi, A. Dimitrakopoulou-Strauss, M. H. Schwarzbach, and L. G. Strauss, "Quantitative, dynamic 18F-FDG-PET for the evaluation of soft tissue sarcomas: relation to differential diagnosis, tumor grading and prediction of prognosis," Hell J Nucl Med, vol. 12, pp. 223-8, Sep-Dec 2009.

[65]   A. Dimitrakopoulou-Strauss, L. G. Strauss, G. Egerer, J. Vasamiliette, G. Mechtersheimer, T. Schmitt, et al., "Impact of dynamic 18F-FDG PET on the early prediction of therapy outcome in patients with high-risk soft-tissue sarcomas after neoadjuvant chemotherapy: a feasibility study," J Nucl Med, vol. 51, pp. 551-8, Apr 2010.

[66]   M. Takesh, "The Potential Benefit by Application of Kinetic Analysis of PET in the Clinical Oncology," ISRN Oncol, vol. 2012, p. 349351, 2012.

[67]   O. C. Hutchinson, D. R. Collingridge, H. Barthel, P. M. Price, and E. O. Aboagye, "Pharmacokinetics of radiolabelled anticancer drugs for positron emission tomography," Curr Pharm Des, vol. 9, pp. 917-29, 2003.

[68]   H. Anderson and P. Price, "Clinical measurement of blood flow in tumours using positron emission tomography: a review," Nucl Med Commun, vol. 23, pp. 131-8, Feb 2002.

[69]   K. Varnas, A. Varrone, and L. Farde, "Modeling of PET data in CNS drug discovery and development," J Pharmacokinet Pharmacodyn, vol. 40, pp. 267-79, Jun 2013.

[70]   P. Zanotti-Fregonara, K. Chen, J.-S. Liow, M. Fujita, and R. B. Innis, "Image-derived input function for brain PET studies: many challenges and few opportunities," J Cereb Blood Flow Metab, vol. 31, pp. 1986 - 1998, 2011.

[71]   Y. Su, A. M. Arbelaez, T. L. Benzinger, A. Z. Snyder, A. G. Vlassenko, M. A. Mintun, et al., "Noninvasive estimation of the arterial input function in positron emission tomography imaging of cerebral blood flow," J Cereb Blood Flow Metab, vol. 33, pp. 115-21, Jan 2013.

[72]   N. A. da Silva, H. Herzog, C. Weirich, L. Tellmann, E. Rota Kops, H. Hautzel, et al., "Image-derived input function obtained in a 3TMR-brainPET," Nuclear Instruments and Methods in Physics Research Section A: Accelerators, Spectrometers, Detectors and Associated Equipment, vol. 702, pp. 22-25, 2/21/ 2013.

[73]   S. Iguchi, Y. Hori, T. Moriguchi, N. Morita, A. Yamamoto, K. Koshino, et al., "Verification of a semi-automated MRI-guided technique for non-invasive determination of the arterial input function in 15O-labeled gaseous PET," Nuclear Instruments and Methods in Physics Research Section A: Accelerators, Spectrometers, Detectors and Associated Equipment, vol. 702, pp. 111-113, 2/21/ 2013.

[74]   A. J. Montgomery, K. Thielemans, M. A. Mehta, F. Turkheimer, S. Mustafovic, and P. M. Grasby, "Correction of head movement on PET studies: Comparison of methods," Journal of Nuclear Medicine, vol. 47, pp. 1936-1944, Dec 2006.

[75]   E. K. Fung and R. E. Carson, "Cerebral blood flow with [15 O]water PET studies using an image-derived input function and," Physics in Medicine and Biology, vol. 58, p. 1903, 2013.

[76]   I. Polycarpou, C. Tsoumpas, A. P. King, and P. K. Marsden, "Impact of respiratory motion correction and spatial resolution on lesion detection in PET: a simulation study based on real MR dynamic data," Physics in Medicine and Biology, vol. 59, p. 697, 2014.

[77] C. Tsoumpas, I. Polycarpou, K. Thielemans, C. Buerger, A. P. King, T. Schaeffter, et al., "The effect of regularization in motion compensated PET image reconstruction: a realistic numerical 4D simulation study," Physics in Medicine and Biology, vol. 58, p. 1759, 2013.

[78] G. Tomasi, S. Kimberley, L. Rosso, E. Aboagye, and F. Turkheimer, "Double-input compartmental modeling and spectral analysis for the quantification of positron emission tomography data in oncology," Physics in Medicine and Biology, vol. 57, p. 1889, 2012.

[79] I. Polycarpou, C. Tsoumpas, and P. K. Marsden, "Analysis and comparison of two methods for motion correction in PET imaging," Medical Physics, vol. 39, pp. 6474-6483, 2012.

[80] P. Zanotti-Fregonara, J. S. Liow, M. Fujita, E. Dusch, S. S. Zoghbi, E. Luong, et al., "Image-derived input function for human brain using high resolution PET imaging with [C](R)-rolipram and [C]PBR28," PLoS One, vol. 6, p. e17056, 2011.

[81] K. C. Schmidt and F. E. Turkheimer, "Kinetic modeling in positron emission tomography," Quarterly Journal of Nuclear Medicine, vol. 46, pp. 70-85, 2002.

[82] P. Zanotti-Fregonara, J. Hirvonen, C. H. Lyoo, S. S. Zoghbi, D. Rallis-Frutos, M. A. Huestis, et al., "Population-Based Input Function Modeling for [F]FMPEP, an Inverse Agonist Radioligand for Cannabinoid CB_1 Receptors: Validation in Clinical Studies," PLoS ONE, vol. 8, p. e60231, 2013.

[83] M. Dahlbom, E. J. Hoffman, C. K. Hoh, C. Schiepers, G. Rosenqvist, R. A. Hawkins, et al., "Whole-Body Positron Emission Tomography: Part I. Methods and Performance Characteristics," J Nucl Med, vol. 33, pp. 1191-1199, June 1, 1992 1992.

[84] R. Hustinx, F. BÈnard, and A. Alavi, "Whole-body FDG-PET imaging in the management of patients with cancer," Sem. Nucl. Med., vol. 32, pp. 35-46, 2002.

[85] K. Kubota, M. Itoh, K. Ozaki, S. Ono, M. Tashiro, K. Yamaguchi, et al., "Advantage of delayed whole-body FDG-PET imaging for tumour detection," European journal of nuclear medicine and molecular imaging, vol. 28, pp. 696-703, 2001.

[86] D. W. Townsend, "Positron Emission Tomography/Computed Tomography," Sem. Nucl. Med., vol. 38, pp. 152-166, 2008.

[87] R. Boellaard, M. J. O'Doherty, W. A. Weber, F. M. Mottaghy, M. N. Lonsdale, S. G. Stroobants, et al., "FDG PET and PET/CT: EANM procedure guidelines for tumour PET imaging: version 1.0," Eur J Nucl Med Mol Imaging, vol. 37, pp. 181-200, Jan 2010.

[88] C. S. Patlak, R. G. Blasberg, and J. D. Fenstermacher, "Graphical evaluation of blood-to-brain transfer constants from multiple-time uptake data.," J Cereb Blood Flow Metab, vol. 3, pp. 1-7, 1983.

[89] M. Reivich, A. Alavi, A. Wolf, J. Fowler, J. Russell, C. Arnett, et al., "Glucose metabolic rate kinetic model parameter determination in humans: the lumped constants and rate constants for [18F]fluorodeoxyglucose and [11C]deoxyglucose," J Cereb.Blood Flow Metab, vol. 5, pp. 179-192, 1985.

[90] G. Blomqvist, S. Stone-Elander, C. Halldin, P. E. Roland, L. Widen, M. Lindqvist, et al., "Positron emission tomographic measurements of cerebral glucose utilization using [1-11C]D-glucose," J Cereb.Blood Flow Metab, vol. 10, pp. 467-483, 1990.

[91] R. A. Brooks, J. Hatazawa, C. G. Di, S. M. Larson, and D. S. Fishbein, "Human cerebral glucose metabolism determined by positron emission tomography: a revisit," J Cereb.Blood Flow Metab, vol. 7, pp. 427-432, 1987.

[92] M. M. Graham, A. M. Spence, M. Muzi, and G. L. Abbott, "Deoxyglucose kinetics in a rat brain tumor," J Cereb.Blood Flow Metab, vol. 9, pp. 315-322, 1989.

[93] S. C. Huang, M. E. Phelps, E. J. Hoffman, K. Sideris, C. J. Selin, and D. E. Kuhl, "Noninvasive determination of local cerebral metabolic rate of glucose in man," Am.J Physiol, vol. 238, pp. E69-E82, 1980.

[94] M. E. Phelps, S. C. Huang, E. J. Hoffman, C. Selin, L. Sokoloff, and D. E. Kuhl, "Tomographic measurement of local cerebral glucose metabolic rate in humans with (F-18)2-fluoro-2-deoxy-D-glucose: validation of method," Ann Neurol, vol. 6, pp. 371-88, Nov 1979.

[95] K. Ho-Shon, D. Feng, R. A. Hawkins, S. Meikle, M. J. Fulham, and X. Li, "Optimized sampling and parameter estimation for quantification in whole body PET," IEEE Trans Biomed Eng, vol. 43, pp. 1021-8, Oct 1996.

[96] C. K. Hoh, C. S. Levin, and D. R. Vera, "Whole body Patlak imaging," J Nuc Med, vol. 51 (Suppl.), p. 61, 2003.

[97] S. K. Sundaram, N. M. Freedman, J. A. Carrasquillo, J. M. Carson, M. Whatley, S. K. Libutti, et al., "Simplified kinetic analysis of tumor 18F-FDG uptake: a dynamic approach," J Nucl Med, vol. 45, pp. 1328-33, Aug 2004.

[98] T. Kaneta, Y. Takai, R. Iwata, T. Hakamatsuka, H. Yasuda, K. Nakayama, et al., "Initial evaluation of dynamic human imaging using F-18-FRP170 as a new PET tracer for imaging hypoxia," Annals of Nuclear Medicine, vol. 21, pp. 101-107, Feb 2007.

[99] J. den Hoff, F. Hofheinz, L. Oehme, G. Schramm, J. Langner, B. Beuthien-Baumann, et al., "Dual time point based quantification of metabolic uptake rates in 18F-FDG PET," EJNMMI Res, vol. 3, p. 16, 2013.

[100] N. A. Karakatsanis, M. A. Lodge, Y. Zhou, R. L. Wahl, and A. Rahmim, "Dynamic whole body PET parametric imaging: II. Task-oriented statistical estimation," Phys. Med. Bio., vol. 58, pp. 7419-7445, 2013.

[101] N. A. Karakatsanis, M. A. Lodge, A. K. Tahari, Y. Zhou, R. L. Wahl, and A. Rahmim, "Dynamic whole body PET parametric imaging: I. Concept, acquisition protocol optimization and clinical application," Phys. Med. Bio., vol. 58, pp. 7391-7418, 2013.

[102] Q. Wang, R. F. Wang, J. Zhang, and Y. Zhou, "Differential diagnosis of pulmonary lesions by parametric imaging in (18)F-FDG PET/CT dynamic multi-bed scanning," J buon, vol. 18, pp. 928-34, Oct-Dec 2013.

[103] N. A. Karakatsanis, Y. Zhou, M. A. Lodge, M. Casey, R. L. Wahl, and A. Rahmim, "Quantitative whole-body parametric PET imaging incorporating a generalized Patlak model," Proc. IEEE Nuc. Sci. Symp. & Med. Imag. Conf., 2013.

[104] N. A. Karakatsanis and A. Rahmim, "Whole-body PET parametric imaging employing direct 4D nested reconstruction and a generalized non-linear Patlak model," Proceedings of SPIE Medical Imaging Conference, 2014.

[105] N. A. Karakatsanis, M. Lodge, R. L. Wahl, and A. Rahmim, "Direct 4D whole-body PET/CT parametric image reconstruction: concept and comparison vs. indirect parametric imaging " J. Nucl. Med., vol. 54 (suppl. 2), p. 2133, 2013.

[106] Z. A. Fayad, V. Fuster, J. T. Fallon, T. Jayasundera, S. G. Worthley, G. Helft, et al., "Noninvasive in vivo human coronary artery lumen and wall imaging using black-blood magnetic resonance imaging," Circulation, vol. 102, pp. 506-10, Aug 1 2000.

[107] J. H. Oo, N. Karakatsanis, A. Rahmim, M. Lodge, and R. Wahl, "A novel imaging method for assessing vessel wall inflammation: Dynamic multi-bed PET parametric imaging," J NUCL MED MEETING ABSTRACTS, vol. 54, pp. 1670-, May 1, 2013 2013.

[108] A. Rahmim, J. Tang, and H. Zaidi, "Four-dimensional (4D) image reconstruction strategies in dynamic PET: beyond conventional independent frame reconstruction.," Med Phys, vol. 36, pp. 3654-3670, Aug 2009.

[109] C. Tsoumpas, F. E. Turkheimer, and K. Thielemans, "Study of direct and indirect parametric estimation methods of linear models in dynamic positron emission tomography.," Med Phys, vol. 35, pp. 1299-1309, Apr 2008.

[110] G. Wang and J. Qi, "Direct estimation of kinetic parametric images for dynamic PET," Theranostics, vol. 3, pp. 802-15, 2013.

[111] R. J. Walledge, R. Manavaki, M. Honer, and A. J. Reader, "Interframe filtering for list-mode EM reconstruction in high-resolution 4D PET," in Nuclear Science Symposium Conference Record, 2003 IEEE, 2003, pp. 2278-2282 Vol.4.

[112] E. A. Jonsson, S. C. Huang, and T. Chan, "Incorporing frame-to-frame coupling in simultaneous reconstruction of dynamic image sequences in PET," in Nuclear Science Symposium Conference Record, 2000 IEEE, 2000, pp. 15/224-15/227 vol.2.

[113] D. J. Kadrmas and G. T. Gullberg, "4D maximum a posteriori reconstruction in dynamic SPECT using a compartmental model-based prior," Phys Med Biol, vol. 46, pp. 1553-74, May 2001.

[114] L. Taek-Soo, W. P. Segars, and B. M. W. Tsui, "Study of parameters characterizing space-time Gibbs priors for 4D MAP-RBI-EM in gated myocardial perfusion SPECT," in Nuclear Science Symposium Conference Record, 2005 IEEE, 2005, pp. 2124-2128.

[115] Z. Bian, J. Ma, L. Lu, J. Huang, H. Zhang, and W. Chen, "Dynamic PET Image Reconstruction Using a Spatial-Temporal Edge-Preserving Prior," Nuclear Science Symposium Conference Record (NSS/MIC), 2013 IEEE,, 2013 2013.

[116] L. Lu, N. A. Karakatsanis, J. Tang, W. Chen, and A. Rahmim, "3.5D dynamic PET image reconstruction incorporating kinetics-based clusters," Phys Med Biol, vol. 57, pp. 5035-55, Aug 7 2012.

[117] A. J. Reader, J. C. Matthews, F. C. Sureau, C. Comtat, R. Trebossen, and I. Buvat, "Iterative Kinetic Parameter Estimation within Fully 4D PET Image Reconstruction," in Nuclear Science Symposium Conference Record, 2006. IEEE, 2006, pp. 1752-1756.

[118] E. Asma, T. E. Nichols, Q. Jinyi, and R. M. Leahy, "4D PET image reconstruction from list mode data," in Nuclear Science Symposium Conference Record, 2000 IEEE, 2000, pp. 15/57-15/65 vol.2.

[119] T. E. Nichols, J. Qi, E. Asma, and R. M. Leahy, "Spatiotemporal reconstruction of list-mode PET data.," IEEE Trans Med Imaging, vol. 21, pp. 396-404, Apr 2002.

[120] J. Verhaeghe, Y. D'Asseler, S. Vandenberghe, S. Staelens, R. Van De Walle, and I. Lemahieu, "ML reconstruction from dynamic list-mode PET data using temporal splines," in Nuclear Science Symposium Conference Record, 2004 IEEE, 2004, pp. 3146-3150 Vol. 5.

[121] J. Verhaeghe, Y. D'Asseler, S. Staelens, and I. Lemahieu, "Optimization of temporal basis functions in dynamic PET imaging.," Nucl Instr Meth A, vol. 569, pp. 425-428, 2006/12/20 2006.

[122] J. Verhaeghe, Y. D'Asseler, S. Staelens, S. Vandenberghe, and I. Lemahieu, "Reconstruction for gated dynamic cardiac PET imaging using a tensor product spline basis.," IEEE Trans Nucl Sci, vol. 54, pp. 80-91, 2007.

[123] J. Verhaeghe, Y. Dasseler, S. Vandenberghe, S. Staelens, and I. Lemahieu, "An investigation of temporal regularization techniques for dynamic PET reconstructions using temporal splines," Med Phys, vol. 34, pp. 1766-78, May 2007.

[124] A. J. Reader, F. C. Sureau, C. Comtat, R. Trebossen, and I. Buvat, "Joint estimation of dynamic PET images and temporal basis functions using fully 4D ML-EM," Phys Med Biol, vol. 51, pp. 5455-74, Nov 7 2006.

[125] A. J. Reader, F. Sureau, C. Comtat, R. Trebossen, and I. Buvat, "Simultaneous Estimation of Temporal Basis Functions and Fully 4D PET Images," in Nuclear Science Symposium Conference Record, 2006. IEEE, 2006, pp. 2219-2223.

[126] J. W. Lin, A. F. Laine, O. Akinboboye, and S. R. Bergmann, "Use of wavelet transforms in analysis of time-activity data from cardiac PET," J Nucl Med, vol. 42, pp. 194-200, Feb 2001.

[127] L. Jou-Wei, A. F. Laine, and S. R. Bergmann, "Improving PET-based physiological quantification through methods of wavelet denoising," Biomedical Engineering, IEEE Transactions on, vol. 48, pp. 202-212, 2001.

[128] P. Millet, V. Ibanez, J. Delforge, S. Pappata, and J. Guimon, "Wavelet analysis of dynamic PET data: application to the parametric imaging of benzodiazepine receptor concentration," Neuroimage, vol. 11, pp. 458-72, May 2000.

[129] F. E. Turkheimer, R. B. Banati, D. Visvikis, J. A. Aston, R. N. Gunn, and V. J. Cunningham, "Modeling dynamic PET-SPECT studies in the wavelet domain," J Cereb Blood Flow Metab, vol. 20, pp. 879-93, May 2000.

[130] J. Verhaeghe, D. Van De Ville, I. Khalidov, Y. D'Asseler, I. Lemahieu, and M. Unser, "Dynamic PET reconstruction using wavelet regularization with adapted basis functions.," IEEE Trans Med Imaging, vol. 27, pp. 943-959, 2008.

[131] A. Rahmim, J. Tang, and H. Mohy-ud-Din, "Direct 4D Parametric Imaging in Dynamic Myocardial Perfusion PET," Frontiers in Biomed. Tech, vol. 1, pp. 4-13, 2014.

[132] E. Tsui and T. F. Budinger, "Transverse section imaging of mean clearance time," Phys Med Biol, vol. 23, pp. 644-53, Jul 1978.

[133] M. A. Limber, M. N. Limber, A. Celler, J. S. Barney, and J. M. Borwein, "Direct reconstruction of functional parameters for dynamic SPECT," Nuclear Science, IEEE Transactions on, vol. 42, pp. 1249-1256, 1995.

[134] M. Bentourkia, "Modeling 13N-ammonia from projections in rat-PET studies," in Nuclear Science Symposium Conference Record, 2001 IEEE, 2001, pp. 1564-1568 vol.3.

[135] J. Matthews, D. Bailey, P. Price, and V. Cunningham, "The direct calculation of parametric images from dynamic PET data using maximum-likelihood iterative reconstruction.," Phys Med Biol, vol. 42, pp. 1155-1173, Jun 1997.

[136] S. R. Meikle, J. C. Matthews, V. J. Cunningham, D. L. Bailey, L. Livieratos, T. Jones, et al., "Parametric image reconstruction using spectral analysis of PET projection data.," Phys Med Biol, vol. 43, pp. 651-666, Mar 1998.

[137] L. Arhjoul and M. Bentourkia, "Assessment of glucose metabolism from the projections using the wavelet technique in small animal pet imaging," Comput Med Imaging Graph, vol. 31, pp. 157-65, Apr 2007.

[138] G. L. Zeng, G. T. Gullberg, and R. H. Huesman, "Using linear time-invariant system theory to estimate kinetic parameters directly from projection measurements," Nuclear Science, IEEE Transactions on, vol. 42, pp. 2339-2346, 1995.

[139] R. H. Huesman, B. W. Reutter, G. L. Zeng, and G. T. Gullberg, "Kinetic parameter estimation from SPECT cone-beam projection measurements," Phys Med Biol, vol. 43, pp. 973-82, Apr 1998.

[140] P.-C. Chiao, W. L. Rogers, N. H. Clinthorne, J. A. Fessler, and A. O. Hero, "Model-based estimation for dynamic cardiac studies using ECT.," IEEE Trans Med Imaging, vol. 13, pp. 217-226, 1994.

[141] P.-C. Chiao, W. L. Rogers, J. A. Fessler, N. H. Clinthorne, and A. O. Hero, "Model-based estimation with boundary side information or boundary regularization [cardiac emission CT]." IEEE Trans Med Imaging, vol. 13, pp. 227-234, 1994.

[142] D. L. Snyder, "Parameter Estimation for Dynamic Studies in Emission-Tomography Systems Having List-Mode Data," Nuclear Science, IEEE Transactions on, vol. 31, pp. 925-931, 1984.

[143] R. E. Carson and K. Lange, "Comment: The EM Parametric Image Reconstruction Algorithm," Journal of the American Statistical Association, vol. 80, pp. 20-22, 1985/03/01 1985.

[144] G. Wang, L. Fu, and J. Qi, "Maximum a posteriori reconstruction of the Patlak parametric image from sinograms in dynamic PET.," Phys Med Biol, vol. 53, pp. 593-604, 2008.

[145] W. Zhu, Q. Li, B. Bai, P. Conti, and R. Leahy, "Patlak Image Estimation from Dual Time-point List-mode PET Data," Medical Imaging, IEEE Transactions on, vol. PP, pp. 1-1, 2014.

[146] J. Tang, H. Kuwabara, D. F. Wong, and A. Rahmim, "Direct 4D reconstruction of parametric images incorporating anato-functional joint entropy," Phys Med Biol, vol. 55, pp. 4261-72, Aug 7 2010.

[147] A. Rahmim, M. Lodge, J. Tang, Y. Zhou, B. Hussain, D. Wong, et al., "Dynamic FDG PET imaging using direct 4D parametric reconstruction in cancer patients," J Nucl Med meeting abstracts, vol. 51, pp. 354-, May 1, 2010 2010.

[148] T. Merlin, P. Fernandez, D. Visvikis, and F. Lamare, "Direct 4D Patlak Parametric Image Reconstruction Algorithm Integrating Respiratory Motion Correction for Oncology Studies," Nuclear Science Symposium Conference Record (NSS/MIC), 2013 IEEE,, 2013 2013.

[149] A. Rahmim, Y. Zhou, J. Tang, L. Lu, V. Sossi, and D. F. Wong, "Direct 4D parametric imaging for linearized models of reversibly binding PET tracers using generalized AB-EM reconstruction.," Phys Med Biol, vol. 57, pp. 733-755, Feb 7 2012.

[150] A. J. Reader, J. C. Matthews, F. C. Sureau, C. Comtat, R. Trebossen, and I. Buvat, "Fully 4D image reconstruction by estimation of an input function and spectral coefficients," in Nuclear Science Symposium Conference Record, 2007. NSS '07. IEEE, 2007, pp. 3260-3267.

[151] W. Guobao and Q. Jinyi, "Direct reconstruction of dynamic PET parametric images using sparse spectral representation," in Biomedical Imaging: From Nano to Macro, 2009. ISBI '09. IEEE International Symposium on, 2009, pp. 867-870.

[152] R. N. Gunn, S. R. Gunn, F. E. Turkheimer, J. A. Aston, and V. J. Cunningham, "Positron emission tomography compartmental models: a basis pursuit strategy for kinetic modeling," J Cereb Blood Flow Metab, vol. 22, pp. 1425-39, Dec 2002.

[153] M. E. Kamasak, C. A. Bouman, E. D. Morris, and K. Sauer, "Direct reconstruction of kinetic parameter images from dynamic PET data," IEEE Trans Med Imaging, vol. 24, pp. 636-50, May 2005.

[154] Y. Jianhua, B. Planeta-Wilson, and R. E. Carson, "Direct 4-D PET List Mode Parametric Reconstruction With a Novel EM Algorithm," Medical Imaging, IEEE Transactions on, vol. 31, pp. 2213-2223, 2012.

[155] Y. Rakvongthai, J. Ouyang, B. Guerin, Q. Li, N. M. Alpert, and G. El Fakhri, "Direct reconstruction of cardiac PET kinetic parametric images using a preconditioned conjugate gradient approach," Med Phys, vol. 40, p. 102501, Oct 2013.

[156] F. A. Kotasidis, A. J. Reader, G. I. Angelis, P. J. Markiewicz, M. D. Walker, P. M. Price, et al., "Direct parametric estimation of blood flow in abdominal PET/CT within an EM reconstruction framework," in Nuclear Science Symposium Conference Record (NSS/MIC), 2010 IEEE, 2010, pp. 2868-2874.

[157] G. Wang and J. Qi, "Generalized algorithms for direct reconstruction of parametric images from dynamic PET data.," IEEE Trans Med Imaging, vol. 28, pp. 1717-1726, 2009.

[158] G. Wang and J. Qi, "Acceleration of the direct reconstruction of linear parametric images using nested algorithms.," Phys Med Biol, vol. 55, pp. 1505-1517, 2010.

[159] W. Guobao and Q. Jinyi, "An Optimization Transfer Algorithm for Nonlinear Parametric Image Reconstruction From Dynamic PET Data," Medical Imaging, IEEE Transactions on, vol. 31, pp. 1977-1988, 2012.

[160] J. C. Matthews, G. I. Angelis, F. A. Kotasidis, P. J. Markiewicz, and A. J. Reader, "Direct reconstruction of parametric images using any spatiotemporal 4D image based model and maximum likelihood expectation maximisation," in Nuclear Science Symposium Conference Record (NSS/MIC), 2010 IEEE, 2010, pp. 2435-2441.

[161] F. A. Kotasidis, J. C. Matthews, A. J. Reader, G. I. Angelis, P. M. Price, and H. Zaidi, "Direct parametric reconstruction for dynamic [18F]-FDG PET/CT imaging in the body," in Nuclear Science Symposium and Medical Imaging Conference (NSS/MIC), 2012 IEEE, 2012, pp. 3383-3386.

[162] G. I. Angelis, J. C. Matthews, F. A. Kotasidis, P. J. Markiewicz, W. R. Lionheart, and A. J. Reader, "Evaluation of a direct 4D reconstruction method using GLLS for estimating parametric maps of micro-parameters," in Nuclear Science Symposium and Medical Imaging Conference (NSS/MIC), 2011 IEEE, 2011, pp. 2355-2359.

[163] P. Gravel and A. J. Reader, "Direct 4D PET MLEM Reconstruction of Parametric Images Using the Simplified Reference Tissue Model with the Basis Function Method," Nuclear Science Symposium Conference Record (NSS/MIC), 2013 IEEE,, pp. M06-1, 2013.

[164] G. Wang and J. Qi, "Direct reconstruction of PET receptor binding parametric images using a simplified reference tissue model," 2009, pp. 72580V-72580V-8.

[165] F. A. Kotasidis, J. C. Matthews, G. I. Angelis, P. J. Markiewicz, W. R. Lionheart, and A. J. Reader, "Impact of erroneous kinetic model formulation in Direct 4D image reconstruction," in Nuclear Science Symposium and Medical Imaging Conference (NSS/MIC), 2011 IEEE, 2011, pp. 2366-2367.

[166] J. C. Matthews, A. J. Reader, G. I. Angelis, P. M. Price, P. J. Markiewicz, and F. A. Kotasidis, "Adaptive parametric kinetic modelling for improved full field of view fitting of PET data," in Nuclear Science Symposium and Medical Imaging Conference (NSS/MIC), 2012 IEEE, 2012, pp. 3925-3929.

[167] F. A. Kotasidis, J. C. Matthews, A. J. Reader, G. I. Angelis, and H. Zaidi, "Application of adaptive kinetic modeling for bias propagation reduction in direct 4D image reconstruction," in Nuclear Science Symposium and Medical Imaging Conference (NSS/MIC), 2012 IEEE, 2012, pp. 3688-3694.

[168] H. Zaidi, N. Ojha, M. Morich, J. Griesmer, Z. Hu, P. Maniawski, et al., "Design and performance evaluation of a whole-body Ingenuity TF PET-MRI system.," Phys Med Biol, vol. 56, pp. 3091-3106, Apr 20 2011.

[169] P. Veit-Haibach, F. P. Kuhn, F. Wiesinger, G. Delso, and G. von Schulthess, "PET-MR imaging using a tri-modality PET/CT-MR system with a dedicated shuttle in clinical routine," MAGMA, vol. 26, pp. 25-35, Feb 2013.

[170] G. Delso, S. Furst, B. Jakoby, R. Ladebeck, C. Ganter, S. G. Nekolla, et al., "Performance measurements of the Siemens mMR integrated whole-body PET/MR scanner.," J Nucl Med, vol. 52, pp. 1914-1922, Dec 2011.

[171] J. Tang and A. Rahmim, "Bayesian PET image reconstruction incorporating anato-functional joint entropy.," Phys Med Biol, vol. 54, pp. 7063-7075, 2009.

[172] L. Caldeira, J. Scheins, P. Almeida, and H. Herzog, "Evaluation of two methods for using MR information in PET reconstruction," Nuclear Instruments and Methods in Physics Research Section A: Accelerators, Spectrometers, Detectors and Associated Equipment, vol. 702, pp. 141-143, 2/21/ 2013.

[173] L. Caldeira, J. J. Scheins, P. Almeida, J. Seabra, and H. Herzog, "Maximum a Posteriori Reconstruction using PRESTO and PET/MR data acquired Simultaneously with the 3TMR-BrainPET," in Nuclear Science Symposium Conference Record (NSS/MIC), 2010 IEEE, 2010, pp. 2879-2884.

[174] K. Vunckx, A. Atre, K. Baete, A. Reilhac, C. M. Deroose, K. Van Laere, et al., "Evaluation of three MRI-based anatomical priors for quantitative PET brain imaging.," IEEE Trans Med Imaging, vol. 31, pp. 599-612, Mar 2012.

[175] H. Wang and B. Fei, "An MR image-guided, voxel-based partial volume correction method for PET images," Med Phys, vol. 39, pp. 179-95, Jan 2012.

[176] J. Tang, H. Kuwabara, D. F. Wong, and A. Rahmim, "Direct 4D reconstruction of parametric images incorporating anato-functional joint entropy.," Phys Med Biol, vol. 55, pp. 4261-4272, Aug 7 2010.

[177] C. Wurslin, H. Schmidt, P. Martirosian, C. Brendle, A. Boss, N. F. Schwenzer, et al., "Respiratory motion correction in oncologic PET using T1-weighted MR imaging on a simultaneous whole-body PET/MR system," J Nucl Med, vol. 54, pp. 464-71, Mar 2013.

[178] M. G. Ullisch, J. J. Scheins, C. Weirich, E. Rota Kops, A. Celik, L. Tellmann, et al., "MR-based PET motion correction procedure for simultaneous MR-PET neuroimaging of human brain," PLoS One, vol. 7, p. e48149, 2012.

[179] Y. Petibon, J. Ouyang, X. Zhu, C. Huang, T. G. Reese, S. Y. Chun, et al., "Cardiac motion compensation and resolution modeling in simultaneous PET-MR: a cardiac lesion detection study," Phys Med Biol, vol. 58, pp. 2085-102, Apr 7 2013.

[180] S. Y. Chun, T. G. Reese, J. Ouyang, B. Guerin, C. Catana, X. Zhu, et al., "MRI-based nonrigid motion correction in simultaneous PET/MRI," J Nucl Med, vol. 53, pp. 1284-91, Aug 2012.

[181] N. Dikaios, D. Izquierdo-Garcia, M. J. Graves, V. Mani, Z. A. Fayad, and T. D. Fryer, "MRI-based motion correction of thoracic PET: initial comparison of acquisition protocols and correction strategies suitable for simultaneous PET/MRI systems," Eur Radiol, vol. 22, pp. 439-46, Feb 2012.

[182] C. Catana, T. Benner, A. van der Kouwe, L. Byars, M. Hamm, D. B. Chonde, et al., "MRI-assisted PET motion correction for neurologic studies in an integrated MR-PET scanner," J Nucl Med, vol. 52, pp. 154-61, Jan 2011.

[183] J. E. Mourik, M. Lubberink, A. A. Lammertsma, and R. Boellaard, "Image derived input functions: effects of motion on tracer kinetic analyses," Mol Imaging Biol, vol. 13, pp. 25-31, Feb 2011.

[184] J. Ouyang, Q. Li, and G. El Fakhri, "Magnetic resonance-based motion correction for positron emission tomography imaging," Semin Nucl Med, vol. 43, pp. 60-7, Jan 2013.

[185] J. U. Fluckiger, X. Li, J. G. Whisenant, T. E. Peterson, J. C. Gore, and T. E. Yankeelov, "Using dynamic contrast-enhanced magnetic resonance imaging data to constrain a positron emission tomography kinetic model: theory and simulations," Int J Biomed Imaging, vol. 2013, p. 576470, 2013.

[186] N. J. Shah, A.-M. Oros-Peusquens, J. Arrubla, K. Zhang, T. Warbrick, J. Mauler, et al., "Advances in multimodal neuroimaging: Hybrid MR–PET and MR–PET–EEG at 3T and 9.4T," Journal of Magnetic Resonance, vol. 229, pp. 101-115, 4// 2013.

[187] E. Poulin, R. Lebel, E. Croteau, M. Blanchette, L. Tremblay, R. Lecomte, et al., "Conversion of arterial input functions for dual pharmacokinetic modeling using Gd-DTPA/MRI and 18F-FDG/PET," Magn Reson Med, vol. 69, pp. 781-92, Mar 1 2013.

[188] R. P. Bokkers, J. P. Bremmer, B. N. van Berckel, A. A. Lammertsma, J. Hendrikse, J. P. Pluim, et al., "Arterial spin labeling perfusion MRI at multiple delay times: a correlative study with H(2)(15)O positron emission tomography in patients with symptomatic carotid artery occlusion," J Cereb Blood Flow Metab, vol. 30, pp. 222-9, Jan 2010.

[189] O. M. Henriksen, H. B. Larsson, A. E. Hansen, J. M. Gruner, I. Law, and E. Rostrup, "Estimation of intersubject variability of cerebral blood flow measurements using MRI and positron emission tomography," J Magn Reson Imaging, vol. 35, pp. 1290-9, Jun 2012.

[190] M. S. J. H. F. Wehrl, F. C. Maier, P. Martirosian, G. Reischl, F. Schick, and B. J. Pichler, "Simultaneous assessment of Perfusion with [15O]water PET and arterial spin labeling MR using a hybrid PET/MR device," in Proc. Intl. Soc. Mag. Reson. Med. 18 (2010), 2010, p. 715.